BEng (Hons) Aeronautical Engineering

Academic Year 2021-2022

ET3107: Project Dissertation

Project Title: *Design of a Turboexpander for Energy Recovery from a Gas let-down station for Blended Natural Gas and Hydrogen Grid*

Student Name: *Abdul-Rahman Asankomah*

Supervisor Name: Dr. Jafar Al-Zaili

Table of Contents

Acknowledgement

I would first like to show my deepest gratitude to my supervisor, Dr. Jafar Al-Zaili, who has supported and guided me throughout my project. Without him, completing my project would not have been possible, and I would not have gained an appreciation for the significant amount of work that goes into turbomachinery design. Dr. Jafar Al-Zaili assisted me in my other academic pursuits as a lecturer in Aerodynamics and Propulsion and has positively contributed to my learning development during my third and final year at the City, University of London. I thoroughly enjoyed spending time with Dr. Jafar, whether that was him as my supervisor, lecturer, or senior mentor when I was a student representative.

I would also like to thank Dr. Youyou Yan, who was my co-examiner and my thermodynamics lecturer in my second year of studies. As the interim Mechanical Engineering and Aeronautics program director, Dr. Yan was extremely approachable, supportive, and eager to assist with any concerns my colleagues and I had.

One of the most exciting challenges as part of my final project was conducting CFD analysis through Ansys. My sincere thanks go to Dr. Mahmoud Khader and Dr. Tala El Samad, who were invaluable in aiding me with understanding some of the technicalities that go into CFD analysis. I would also like to thank Dr. Omar Selim for always lighting the room with his beaming smile and providing an engaging and enriching learning experience through his software tutorials in my second year of studies.

A debt of gratitude is also owed to my A-level Physics teacher, Mr. Zamir Khaliq, without whom I would not have developed the self-belief to enrol on this challenging yet rewarding course. I will never forget the times he challenged my mindset and revealed what was possible if I would only set my mind to it.

Finally, I would like to thank my family, friends, and colleagues. Engineering is not something one can do alone, and I sincerely believe I could not have completed my degree without you all, so thank you.

Nomenclature and Acronyms

A	Area [m^2]
D	Diameter [m]
V	Velocity [m/s]
ρ	Density [kg/m^3]
U	Blade Speed [m/s]
N	Rotational Speed of Impeller [rpm]
w	Relative fluid velocity [m/s]
c	Absolute fluid velocity [m/s]
h	Specific Enthalpy [KJ/kg]
W	Specific work [KJ/kg]
Q	Heat transfer [KJ/kg]
Re	Reynolds Number
T	Temperature [K]
η	Efficiency
$\dot{m}$	Mass flow rate [kg/s]
E	Energy [KJ]
r	Radius [m]
s	Entropy [KJ/Kg K]
Ω_s	Specific speed [rad]
N_s	Dimensionless specific speed
P	Pressure [Pa]
P_r	Pressure ratio
IFR	Inward-Flow Radial
PRS/GRS	Pressure/ Gas Regulation Station
δ	Boundary-Layer thickness [mm]
X	Mass fraction
C_p	Specific heat (Pressure = const.)
C_v	Specific heat (Volume = const.)
K	Specific heat ratio
R	Gas Constant [KJ/kgK]
M	Molar mass [kg/kmol]

Subscripts

0	Total Property at stagnation
1-4	Turbine state points
r	Rotor
rel	Relative
T-t	Total-to-total
T-s	Total-to-static
s	Isentropic
NG	Natural Gas
H	Hydrogen
N	Nozzle

List of Figures

List of Tables

1 Abstract

This investigation carried out the design and numerical analysis of several 90° IFR turbines optimized for different hydrogen and natural gas blends to evaluate their performances. After researching the thermodynamics of the turbine, a mean line design of a given turbine blade profile was initiated using Ansys Vista RTD. Afterwards, a 3D model of the turbine blade with fluid passage was generated using BladeGen. The inlet and outlet flow angles were optimized in BladeGen to increase the performance of the turbine. TurboGrid was then used to create a computational grid and optimize the blade and fluid passages mesh. Finally, Ansys CFX was used to carry out the 3D numerical simulation, where the Shear Stress Transport (SST) turbulence model was selected. It was discovered that the 1D and 3D results compared well for the majority of the CFD turbine geometric designs and that a turbine designed using 10% hydrogen would offer the best performance for a gas grid operating with a hydrogen and natural gas blend.

Keywords: Radial Turbine, Hydrogen, BladeGen

2 Introduction and Background

With the advent of COP26, there has not been a more critical time than now to adopt efficient ways of producing energy and reducing harmful emissions. The gas grid is an essential and highly integrated infrastructure for the transport of natural gas through countries worldwide. The network consists of gathering systems, gas processing plants, wide diameter transmission pipelines, and small diameter low-pressure service lines. In 2020 alone, the natural gas transportation network in the U.K delivered over 27.7 trillion cubic feet of natural gas to almost 21 million homes. Unfortunately, the process through which the pressure of the gas is lowered before distribution is energy inefficient as the kinetic energy of the working fluid is not made well use of. Loses of up to 7.5MW have been recorded at some Gas Regulation Stations (GRS). In place of a pressure valve, turboexpanders are proposed to recover some of the pressure energy, which can then be used to generate electricity. Hydrogen can be injected into the grid as a method to reduce the combustion of methane. Due to end-user systems constraints, the existing turbomachine blade designs cannot accommodate a blended network. Thus, this project will focus on generating blade designs for different blend ratios and recommend the most efficient design. To capture the blade design requirements, the operating thermodynamic conditions of a typical gas let-down station will be utilized. The GRS operating conditions will also allow investigation into how the design will work under actual boundary conditions. CFD is a powerful tool that will be used to assess how the turbine would operate in different gas blend cases involving hydrogen and natural gas.

As shown in Fig. (2.1), a gas grid is an integrated network of objects and systems to transport and distribute natural gas. The components include underground natural gas storage, compressor stations, Gas Regulation Stations (GRS), and gas pipelines (Szoplik, 2012). The gas compression process is required as the gas loses pressure after traveling for long distances in the pipes. The component of interest in this project is the GRS, of which several types can be considered. GRS stations are characterised by various parameters and can broadly be divided into high-pressure reduction, middle-pressure reduction, metering, and distribution stations. Szoplik (2012) highlights the pressure characteristics of each gas pipeline system, where the middle-pressure reduction stations supply natural gas in the order of $\sim 1\ MPa$ for industrial and commercial uses. Since these types of middle-pressure reduction stations are essential to the economy, the turbomachinery design will be made to operate at these types of stations.

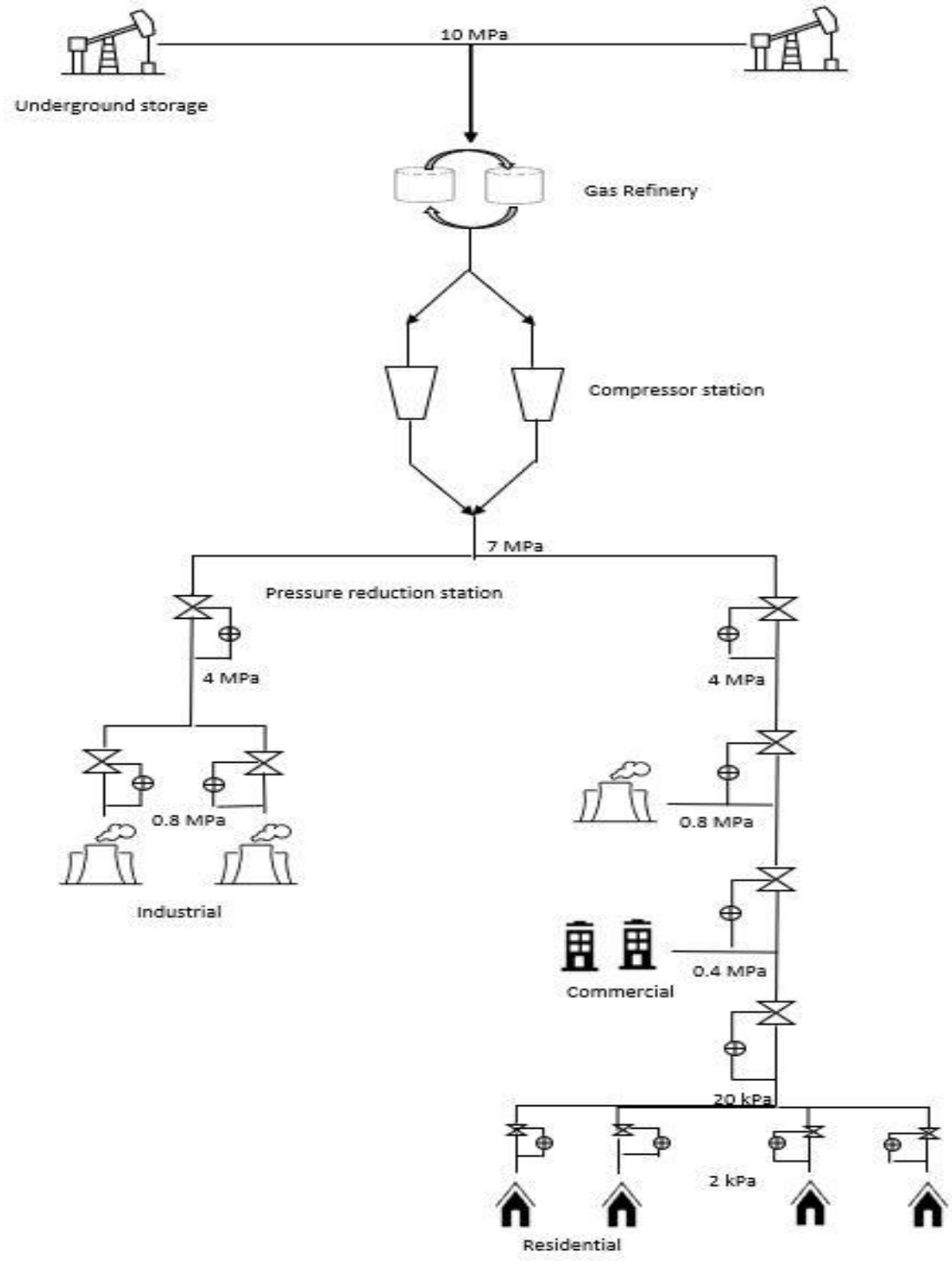

Figure 2. 1: *A typical Natural Gas Distribution Network (made via Microsoft Visio and Word)*

The use of valves such as Joule-Thompson valves for pressure reduction still dominates in most pressure-reducing stations. This method of pressure regulation is inefficient as it involves energy dissipation that results in irreversible losses in the gas stream (Kuczynski et al., 2019a). Moreover, electricity consumption increased by 743% between the early 80s and 2010 (Neseli, Ozgener, and Ozgener, 2015). Thus research based on boosting productivity in energy production can play a critical role in energy recovery. From this standpoint, this project is of great importance.

Over 180 years ago, the radial flow turbine, the outflow type, was first conceived for hydraulic power generation. A much highly regarded turbine, mainly due to the thermodynamic benefits associated with the flow path, is the radial-inflow type, developed in 1847 by Francis and Boyden in the USA. The inward-flow radial (IFR) turbine is flexible due to the ranges of power it can cover, mass flow rates, and rotational speeds. This makes them an excellent choice to use in turbomachines at gas let-down stations as they could extract more work from the working fluids and are generally easier to manufacture, making them scalable.

Of the two main types of IFR turbines, namely the 90^{o} IFR and cantilever turbine, the latter requires an increased inflow area resulting from the rotor expansion, which is difficult to accommodate (Dixon and Hall, 2010). The 90° IFR has greater structural strength than the cantilever entailing that the rotor vanes can accommodate high-stress levels induced by centrifugal forces. Thus, they would be the focus of this design enterprise.

3 Literature Review

3.1 The utilisation of Turboexpanders in existing GRS

Turboexpanders are rotating devices that convert the pressure energy of gases into mechanical work. From several case studies observed, GRS stations that are eligible to have a turboexpander installed have reaped the benefits of gas pressure reductions and energy recovery. Neseli, Ozgener, and Ozgener, (2015) found that 23% of the energy used in compressor stations was recovered at a gas station in Takestan, Iran. Different types of turbines have been investigated, such as axial impulse turbines (Morgese et al., 2020). The methodology used by Morgese et al., (2020) at a GRS in Austria is innovative and can be extrapolated to the design of radial turbines in this project. A fundamental design process is laid out by (Dixon and Hall, 2010), which goes into the thermodynamic equations used for the main components of the turbine, such as the nozzle, stator, rotor, and diffuser. After defining the turbine design point, the mass flow rate,$\dot{m}$, and boundary conditions such as the inlet and outlet temperatures and pressure can be obtained. The losses

in the 90-degree IFR turbine can be analysed to account for irreversibility. The primary geometric parameters and specifications, such as the rotor diameter and inlet and outlet flow angles, can then be estimated from a 1D analysis. An optimisation algorithm in Ansys defines the 2D blade profile, and a 3D CFD simulation is carried out to compute the efficiency. Sam and Ghosh, (2017) utilised Ansys CFX to analyse the flow field of a helium turboexpander, which aided in improving the efficiency of these technologies. Fig. (5.4) shows a limited range of specific speeds that can produce a high-efficiency turbine. This performance correlation can also be used to check the final design.

The temperature drops per MPa when expansion turbines are used are more significant than traditional pressure regulators (Požívil, 2004). The exit temperature of the turbine must not be too cold to avoid the pipes being brittle and to avoid sulphates from forming. For the exit temperature to be $\sim 300°K$ (ambient temperature) and equal to the inlet temperature, several methods have been proposed. This gas can either be preheated or heated at the exit using the energy generated from the turbine. The former approach has been explored in great depth. Farzaneh-Gord et al., (2012) examined a solar system method of preheating, which can decrease the capital cost that is usually high at stations where boilers are utilised.

Furthermore, Villecco and Pellegrino, (2010) showed that the device's efficiency could be affected by variabilities and irregularities in boundary conditions. Fig. (3.2) shows a schematic of a gas reducing station where a turboexpander is installed parallel with a traditional reduction station. This arrangement proposed by Kuczynski et al., (2019a) is to cater for off-design operations of the turbine. However, by bypassing some of the flow through a traditional expansion valve, electricity cannot be generated, which would defeat the purpose of this project’s enterprise. There are other proposed mechanisms of dealing with this issue. Turbines are usually less sensitive to variation of mass flow rate than compressors, thus over a relatively wide range of operation, the turbine can still operate at a high efficiency. There are several other considerations such as having a parallel turbine arrangement however, the detailed calculations regarding the off-design operation are out of scope of this project.

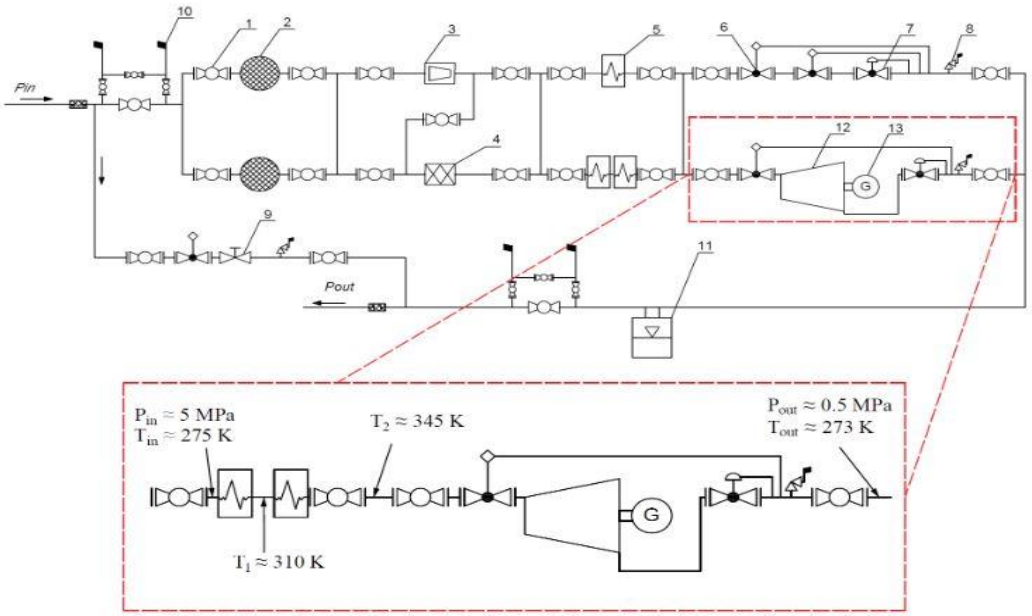

Figure 3. 1: *Turboexpander parallel arrangement with a traditional expander at a GRS (Kuczynski et al., (2019a))*

Installing a turboexpander is a considerable investment, and there are several ideas to keep in mind. Wherever it is possible, efficiency should be improved, which is becoming more critical due to imperatives and legal requirements in some countries. That said, funding to deploy the technology on a wide scale is challenging. Furthermore, there are also some safety implications with installing and using a turboexpander. The electrical generator close to the pipeline should be fully sealed such that in case of any spark, there are no explosions.

3.2 Turboexpanders for hydrogen applications

Currently, 84% of homes in the U.K. receive their energy supply from a natural gas pipeline network. The U.K. Climate Change Act 2008 requires the country to decrease 80% GHG emissions by 2050. Several options have been investigated to reach this goal. An important future energy carrier is hydrogen, which is proposed to lower GHG emissions significantly, mainly when produced from low carbon sources (Kuczynski et al., 2019b). Based on the system's existing natural gas characteristics and end-user constraints, an option suggested by Dodds and McDowall, (2013) and is to inject small amounts of hydrogen into the gas network. Kuczynski et al., (2019b) found that the maximum participation of hydrogen in natural gas should not exceed the range of 15% to 20% by volume. This limit is also consistent with other authors such as Witkowski et al., (2018). Melaina, Antonia and Penev, (2013) also suggested a range of 5% to 20% of hydrogen by volume without increasing associated risks. An analysis using the MARKAL optimisation algorithm indicates that the maximum

amount of hydrogen should be introduced by 2035 to reach decarbonization goals by 2050 (Dodds and McDowall, 2013).

In terms of computing blended ideal gas thermodynamic properties, Balmer and Robert T, (2011) demonstrated a straightforward method that can be used. The mass fractions for each blend can be calculated to compute parameters such as the gas constant, which can then be imported to Ansys CFX-pre. The radial expander will be designed to operate at a medium-pressure reduction station in the Czech Republic for this project. Unlike the work done by Požívil, (2004), the turbine would be designed to consider a natural gas and hydrogen gas blend to analyse the effect this has on the performance of the expander.

4 Aim and Objectives

This project will explore the performance of a 90° IFR turbine that utilises a natural gas and hydrogen blend. This project can help deepen the understanding of the performance of a turbine that utilises a blended gas as a working fluid and offer a potential design option for the future goal of incorporating hydrogen in the gas grid. The rationale for this turboexpander design is to convert electricity from renewables to hydrogen at low-demand, high energy production periods such as during the day for solar cells. This can be achieved by electrolysing water and injecting the hydrogen into the pipelines so that when demand is high, and production is low, the hydrogen-natural gas blend can be converted back to electricity.

4.1 Objective 1: Obtain the idiosyncratic radial turbine parameters

Radial turboexpanders possess distinctive characteristics thus, an applicable method is needed for their design. The radial turboexpander in this project will be working with compressible gases thus, a zero-dimensional analysis will be required to capture the fluid mechanics and thermodynamic requirements. As with any turbomachine, losses are present, and design constraints must not be violated to obtain a useful product at the end of the process. By the end of this objective, a thermodynamic model will be made, which contains an initial estimate of the total-to-static efficiency, η_{T-s} of the turbine.

4.2 Objective 2: Realize a suitable case study

With clarity on the thermodynamic requirement gained from the first objective, research can be made into existing GRS to characterize the radial expander design. It is essential to find a case study where a turboexpander has been used to replace a conventional pressure reduction valve. Parameters of interest at this stage are the efficiencies and boundary conditions such as the inlet and outlet pressures and temperatures. By means of a suitable simulation and 3D design software such as Ansys, the thermodynamic model developed from objective one will be converted into a 1D model. The 1D model will be used to predict various properties such as the total-to-static efficiency, the inlet and outlet diameter, and velocity triangles. A first milestone will be when a natural gas 1D model has been made and analysed utilising CFD using an appropriate mesh from Ansys TurboGrid. The CFD is a way to evaluate the turboexpander performance, which will be compared against initial estimations.

4.3 Objective 3: Identify acceptable gas blends

After analysing a purely natural gas design, gas blends with hydrogen will be investigated. Due to limitations in the extent of gas blends, the range of blends that will be analysed will not exceed 15% to 20% of hydrogen by volume. Consequently, the number of cases that will be studied will be limited to three. Anything less than three may be insufficient, and anything above that may be time-consuming and unnecessary to convey the implications of blended designs. A second milestone will be when all three cases have undergone a CFD analysis with the appropriate meshing.

5 Methodology

Fig. (5.1) summarises the proposed analysis method in the form of a flowchart. The nominal design point was defined after conducting a literature review and reading various thermodynamics and radial design books. The governing thermodynamic equations for the rotor form the backbone of the engineering design in this project. The operating conditions such as the mass flow rate, $\dot{m}$, the temperature, T and pressure ratio, P_r, and rotational speed, N, were defined at this stage. The values were coded in Excel and MATLAB.

The isentropic efficiency was coded into Ansys Vista RTD, using a trial value as an initial estimate. After that, the other aerodynamic and geometrical constraints were defined and implemented into the software to obtain the 1D model. The output of this analysis yields the flow angles and total-to-static efficiency, among other parameters. Subsequently, BladeGen can be used to produce and refine the meridional profile and the 3D geometrical model of the blade, which can later be transported to TurboGrid for meshing. Finally, the simulation settings and gas parameters can be defined in Ansys CFX-pre, followed by a CFD analysis. To reach a satisfactory turbine design, iterations are necessary until convergence is reached. The iteration stops when the efficiency from the CFD analysis is maximized and is comparable with the value produced from Vista RTD. At the end of this step, the results obtained provide the geometric and aerodynamic parameters to construct the turbine. The hydrogen volume in natural gas blends that will be investigated are 5%, 10%, 15% and 20%. The design process was accomplished based on the predefined parameters such as the total inlet temperature, total inlet pressure, mass flow rate, and pressure ratio, which constitute the boundary conditions.

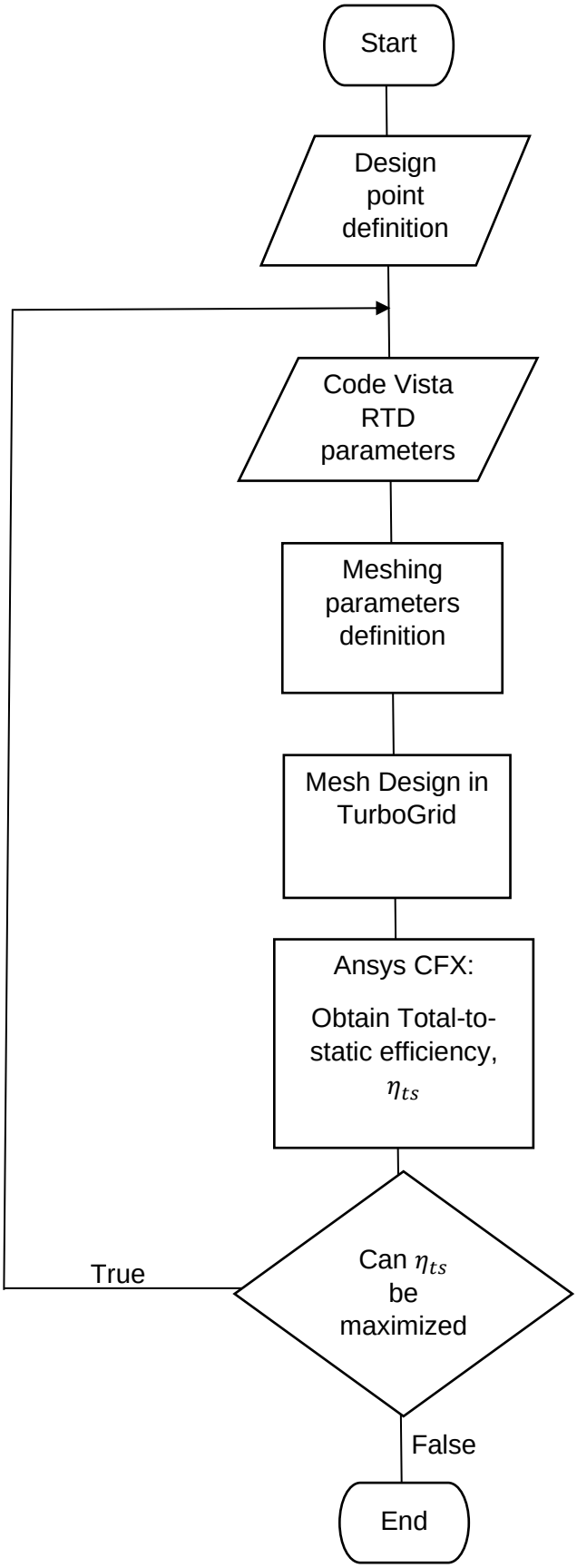

Figure 5. 5: *Flowchart for the method of analysis*

5.1 Zero-dimensional Analysis of a 90° IFR turbine

The properties of interest that define the thermodynamic state of an ideal fluid include pressure and temperature and velocity and flow angles. Fig. (5.2) shows a typical layout and associated velocity diagrams of a 90-degree IFR turbine. The stations are explained as follows:1 – nozzle inlet, 2 – nozzle exit/ rotor inlet, 3 – rotor exit/diffuser inlet, 4 – diffuser exit.

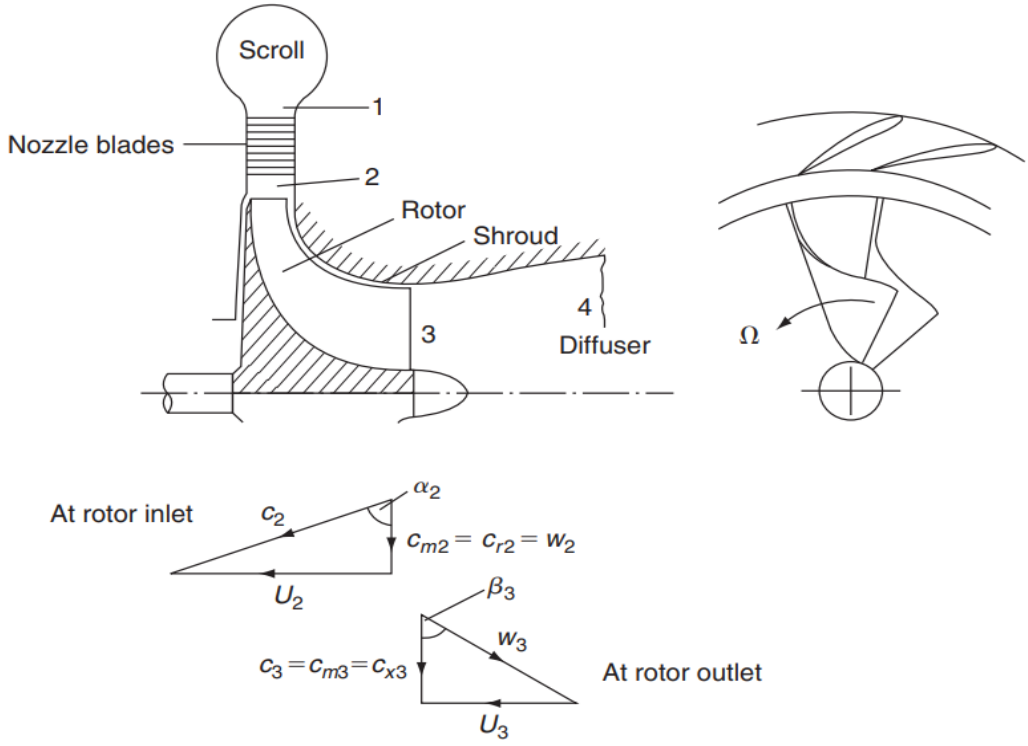

Figure 5. 6: *Layout and Velocity Diagram representing the nominal design condition for a 90-degree IFR Turbine (Dixon and Hall, 2010, p.268)*

The fluid enters station one with an absolute velocity of c_1. where it is accelerated by the nozzle to a higher absolute velocity of c_2. The flow moves into station two with a radial velocity of w_2, which is at an angle of α_2 to c_2. The rotational speed of the rotor is Ω and U_2 is its tangential tip velocity. At station two, the rotor vanes extend radially inward and turn the flow through a 90-degree turn, a fluid deceleration process. At station three, the gas exits the turbine axially with an absolute speed of C_3 and enters the diffuser with a flow angle of β_3 and a radial velocity, w_3. The tangential speed of the rotor is different and is equal to U_3. The flow eventually exists in the diffuser at station four.

For all intents and purposes, the flow will also be considered steady thus, the continuity equation can be invoked to develop a relationship between rotor inlet and outlet conditions:

$$\dot{m} = \rho_2 * w_2 * A_2 = \rho_3 * w_3 * A_3 = constant \quad (1)$$

From an energy balance of a system (first law of thermodynamics), the net change in the total energy during a process is equal to the total energy entering the system and the total energy leaving that system (Cengel, Boles, kanoglu,2018):

$$E_{in} - E_{out} = \Delta E_{system} \quad (2)$$

Eqn. (2) gives rise to steady flow energy equation, Eqn. (3), which needs to be considered as a logical design starting point since a rotor is essentially a work transfer device (Whitfield and Baines, 1990).

$$\frac{\dot{Q}}{\dot{m}} - \frac{\dot{W}}{\dot{m}} = (h_2 - h_1) + \frac{1}{2}(C_2^2 - C_1^2) + g(z_2 - z_1) \quad (3)$$

For the turbomachines being considered, the potential energy term is negligible.

Applying the adiabatic condition to Eqn. (3), and making the appropriate sign changes for a turbine (since the heat in is zero) yields:

$$\frac{\dot{W}}{\dot{m}} = \left(h_1 + \frac{1}{2} C_1^2\right) - \left(h_2 + \frac{1}{2} C_2^2\right) = (ho_{in} - ho_{out}) = C_p\left(T_{0,in} - T_{0,out}\right) \quad (4)$$

Furthermore, the specific work on the rotor by the fluid is given by the Euler turbomachinery equation below, Eqn. (5). This equation can be manipulated using the velocity triangles to define the work transfer per unit mass from station one to three in terms of rotor and fluid velocities, Eqn. (6):

$$\Delta W = h_{01} - h_{03} = U_2 C_{\theta 2} - U_3 C_{\theta 3} \tag{5}$$

Since the stagnation enthalpy across the nozzle is constant $h_{01} = h_{02}$, Eqn. (5) can be manipulated to obtain Eqn. (6):

$$\Delta W = h_{02} - h_{03} = \frac{1}{2}[(U_2^2 - U_3^2) - (w_2^2 - w_3^2) + (C_2^2 - C_3^2)] \tag{6}$$

All three terms in Eqn. (6) contribute to the specific work output. Since the first term is positive for a turbine as $U_2 > U_3$, it translates into a more significant energy extraction from the fluid turbine than the axial turbine where $U_2 = U_3$.

The Mollier diagram, Fig. (5.3), illustrates the expansion process for the IFR turbine layout shown in Fig. (5.2). The expansion process is ideally one that is irreversible and adiabatic between stations two and three. However, there is an increase in entropy from stations two to three, as indicated by Eqn. (7):

$$s_3 > s_2 \tag{7}$$

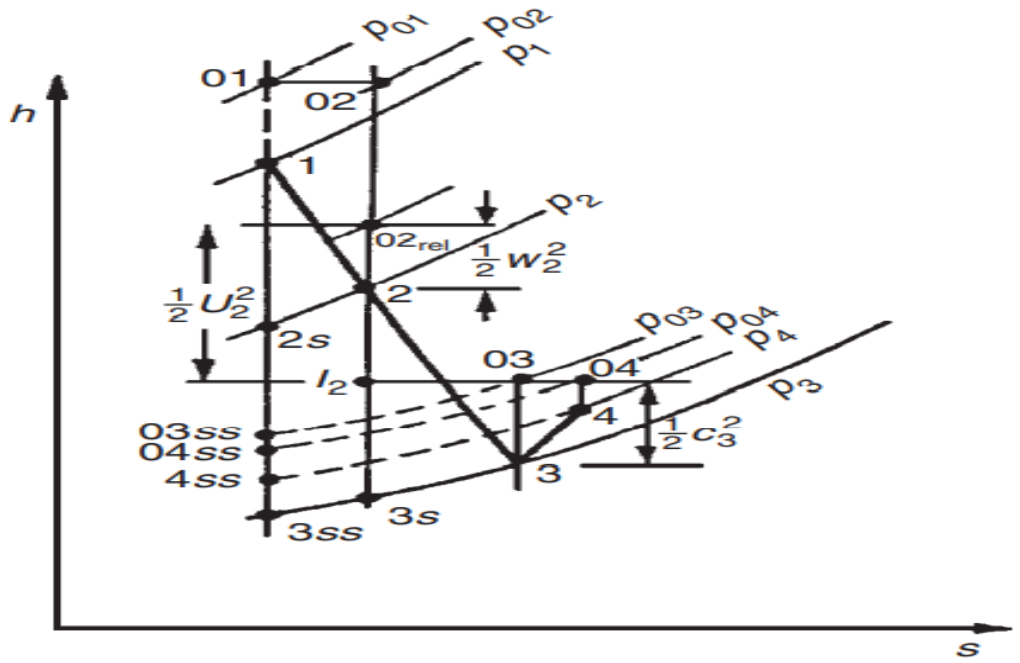

Figure 5. 7: *Mollier Diagram for 90- degree IFR Turbine (Dixon and Hall, 2010, p.269)*

The work output can be made a simple function of blade speed only through Eqn. (8), by setting the flow angle at the inlet relative to the blade equal to zero and assuming the exit velocity from Eqn. (5) is axial.

$$\Delta W = U_2^2 \tag{8}$$

One of the most important parameters of turbomachinery design is efficiency. For an expander, this is generally defined as:

$$\eta_T = \frac{Actual\ work\ output}{Work\ output\ in\ an\ ideal\ process\ between\ two\ defined\ end\ states} \tag{9}$$

The efficiency will be defined using station one, the stagnation state (since this is where the fluid has maximum kinetic energy), and station three, the outlet. The ideal process of interest will be isentropic as the expansion process is considered adiabatic. Within this definition, the efficiency will only consider blade losses and exit

kinetic energy internal losses of the fluid. Thus, for a turbine operating on an ideal gas and for $T_1 > T_2$:

$$\eta_{T-s} = \frac{h_{01} - h_{03}}{h_{01} - h_{3s}} \tag{10}$$

$$\eta_{T-s} = \frac{W_{actual}}{W_{ideal}} = \frac{\dot{m}C_p(T_1 - T_2)}{\dot{m}C_p(T_1 - T_2')} = \frac{T_1 - T_2}{T_1 - T_2'} \tag{11}$$

In turbomachinery design, there are two main types of efficiency to investigate: the total-to-total and total-to-static efficiencies, of which the latter is usually higher than the former. The isentropic efficiency given by Eqn. (11) is of prime importance in this investigation as the flow at the exit should have some kinetic energy that should be as low as possible without reaching zero. A typical value for an IFR turbine operating at a gas let-down station is about η_{Ts} = 80-85%. Rohlik, (1968) discovered that there a limited range of specific speed, N_s, that can a produce a turbine that has high isentropic efficiency: the value should lie between 0.3 and 0.6, according to Fig. (5.4). Since this turbine is to be designed for the highest efficiency, the efficiency value that corresponds to 0.3, that is 80%, would be used and later verified in Vista RTD. At the best efficiency point of actual (frictional) 90° IFR turbines, it is found that this velocity ratio is, generally, in the range of $0.68 < U_2/c_0 < 0.71$, where c_0 is known as the spouting velocity (Dixon and Hall, 2010).

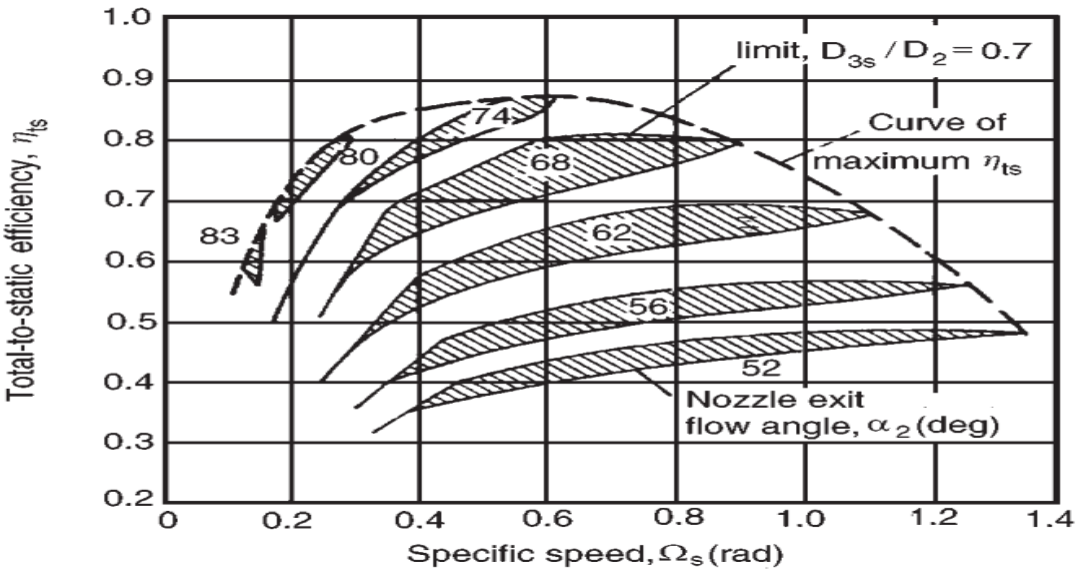

Figure 5. 8: *90 degrees IFR turbine performance (Dixon and Hall, 2010, p.269)*

In an early study of IFR turbine design for maximum efficiency, Rohlik, (1968) specified that the ratio of the rotor shroud diameter to rotor inlet diameter should be limited to a maximum value of 0.7 to avoid excessive shroud curvature and that the exit hub–shroud tip ratio to be set to a minimum of 0.4 to avoid excess hub blade blockage and loss.

5.2 Preliminary 1D design

The turbine operating parameters for natural gas was obtained from a middle-pressure GRS in Velké Němčice, Czech Republic, and tabulated in Table (5.1). Since a one-dimensional flow is of concern in this analysis, it was assumed that the trajectory of the fluid is along streamlines that follow the geometry of the blades. Any slight deviations were considered negligible. Vista RTD is a radial turbine preliminary design tool that allows users to specify aerodynamic and geometric design inputs and returns the blade meridional profile and the analysis results. The results of interest include the η_{T-S}, N_s, D, inlet, and outlet flow angles and the velocity diagrams. Since supersonic conditions should be avoided in the turbine to prevent a decrease in performance, the blades were optimized iteratively to obtain ~ Mach 1 at the inlet and a Mach number "1 at the outlet, which should be the case for a well-designed rotor. For optimal performance, the exit absolute tangential velocity should be ideally zero. However, in practical applications, it is reasonable to assume that the absolute Mach number at the rotor exit has a relatively low value.

Thus, the turbine's efficiency was maximized by optimizing the inlet and flow angles such that the relative in-flow angle and the absolute flow angles were as close to zero as possible. The resulting velocity diagrams can be seen in Fig. (6.2).

Table 5. 1: *Specified Aerodynamic parameters for Vista RTD*

Inlet Stagnation Temperature [℃]	Inlet Stagnation Pressure [MPa]	Mass flow rate [kg/s]	Expansion ratio
300	5.5	11.3	3.1

The blade speed ratio (U_2/c_0) and total-to-total efficiency inputs were optimized in such a way to maximize the total-to-static efficiency of the turbine. The nozzle efficiency, η_N, was maintained at the default value of 0.9 as it is representative of many radial in-flow turbine designs (Michal, 2013).

The number of blades was optimized by utilizing Eqn. (12), the modified Jamieson expression made by Glassman, (1976). The initial Jamieson expression is shown in Eqn. (13) yielded too many blades, however using Eqn. (12) decreases the number of blades required in each design without degrading the performance of the design (Glassman, 1976).

$$n_r = \frac{\pi}{30}(110° - \alpha_2)tan(\alpha_2) \tag{12}$$

$$n_r = 2\pi tan(\alpha_2) \tag{13}$$

5.3 Energy Analysis

The use of an expansion turbine requires an energy analysis for many reasons. For instance, the gas temperature must remain above the hydrate zone and dew point (≅ 258K) to prevent the pipes from becoming brittle, which could lead to structural failures (Maddaloni and Rowe, 2007).Two methods of overcoming this problem is to either use some of the recovered energy to preheat the gas (before it enters the turbine inlet) or post-heat the gas at the exit so that it is close to the inlet temperature. The energy-efficient process will be discovered following the analysis and recommended as the option to consider. For both cases, the temperature of the gas entering the GRS is 300K, and the temperature of the gas leaving the GRS is 290K and there are some variables that must remain fixed, namely the η_{T-S}, P_r, and $\dot{m}$.

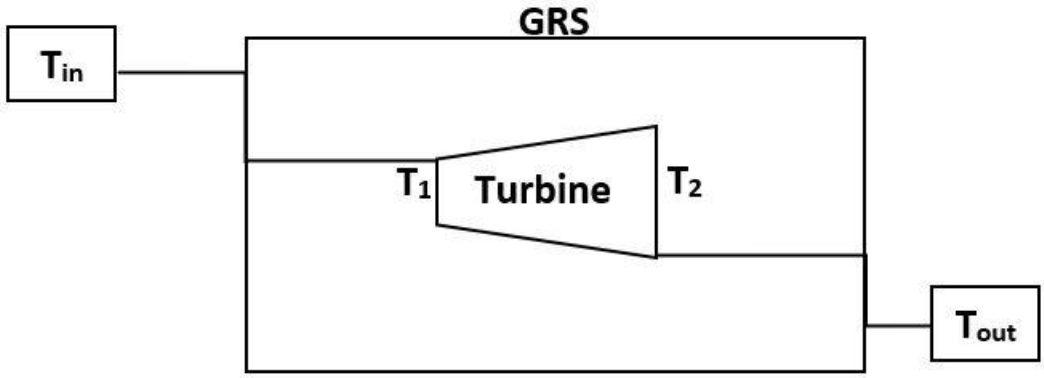

Figure 5. 9: *Rudimentary sketch showing the temperature in the gas pipelines that enter & leave the station, T_{in} and T_{out}, and the temperature that goes into and leaves the turbine, T_1 & T_2.*

From Fig. (5.5), an isentropic expansion in the turbine can be considered, which leads to the following equation:

$$\left(\frac{T_2'}{T_1}\right) = \left(\frac{P_2}{P_1}\right)^{\frac{\Upsilon-1}{\Upsilon}} \tag{14}$$

The heat energy required to heat the fluid is given by:

$$\dot{q} = \dot{m}\overline{C_p}\Delta T \tag{15}$$

The variable $\overline{C_p}$ is an average value obtained by finding the average temperature and substituting it into the polynomial function of C_p, which is shown in the MATLAB code in the appendix. In the case of preheating, T2 is fixed,where $T_2 \approx T_{out} \cong 290K$. T_2' and T_1 are unknown, however Eqn. (11) and (14) can be manipulated to determine the value of T_1 by forming a relationship between T_1 and T_2'. For post-heating, T_1 is fixed and $T_1 \approx T_{in} \cong 300K$. After determining the heat required to heat the fluid using Eqn. (15), the power of the turbine and net power could be calculated using Eqn. (16) and (17) respectively. The specific power was also obtained from Eqn. (18). The computation was completed using MATLAB, and the results are summarised in Table (6.4) for both heating options.

The power that can be extracted from the turbine is:

$$\dot{W}_T = \dot{m}\overline{C_p}(T_1 - T_2) \tag{16}$$

The net power is given by:

$$\dot{W_{net}} = \eta_{mechanical} * W_T * \eta_p - \dot{q} \tag{17}$$

The specific power is given by:

$$\Delta W = \frac{\dot{W}}{\dot{m}} \tag{18}$$

At the turbine exit, a mass flow rate is still needed thus, kinetic energy cannot be zero at that point. However, the absolute velocity at the exit, V_3, must be minimized as much as possible otherwise, a high energy flow would increase the losses. This is the justification for using total-to-static efficiency over total to-total as the former factorizes the kinetic energy of the fluid at the exit.

5.4 Gas Blend Cases

By utilising the chemical properties of both natural gas and hydrogen, mass fraction calculations were executed in MATLAB to derive the properties of the blended gas cases. The percent volume of each mixture for the different cases was multiped by their respective molar masses and was added to determine the molar mass of the mixture. A line of code was included to ensure that the summation was added to unity after each calculation. The mixture composition on a mass basis was then determined, which enabled other equivalent parameters to be computed, such as the specific heat at constant pressure, gas constant, and density. The thermodynamic properties of the gases used are summarized in Table (5.2), and the results of the mass fraction calculations can be found in Table (6.5). Five different geometries were constructed in Vista RTD, each based on a distinct gas blend. Each geometry was then made to operate on the five different gas blends shown in Table (6.5) to see how this would affect their performance.

Table 5. 2: *Gas properties of interest*

Gas	Gas Formula	ρ [kg/m^3]	C_p [KJ/KgK]	C_v [KJ/KgK]	k	R [KJ/kgK]	M [kg/kmol]
Hydrogen	H_2	0.0838	14.301	10.183	1.405	4.124	2.016
Methane	CH_4	0.668	2.254	1.7354	1.299	0.5182	16.043

5.5 Grid Generation and Mesh

TurboGrid was used due to its capability to provide high-quality mesh for complex blade geometries. The impeller's geometry was transferred from BladeGen to TurboGrid. A turbine blade in the software is represented as a single periodic section, and a set of geometric regions is created automatically, namely the inlet, passage, shroud, hub, and outlet (ANSYS, 2015). The Automated Topology and Meshing (ATM) option was enabled to robustly create a mesh such that modification of the mesh control points would be avoided. The topology affects how the mesh is made and directly influences the mesh quality. The topology set object was

unsuspended to automatically create the full 3D hexahedral mesh. The user can control the number of elements and nodes through means such as increasing the size factor, which has the effect of increasing total elements and decreasing the first layer thickness.

A vital flow phenomenon to capture is the boundary layer, which varies in thickness, δ of the order ~1mm, around the blade profile. The boundary layer arises due to viscous effects, which result in momentum losses, affecting the efficiency of the turbine blades. The boundary layer has several properties controlled using the boundary layer refinement control and selecting a suitable method from the options. The near-wall element size speciation allows the user to control the spacing distance between the blade and the first layer of nodes from the wall. The y^+method was utilised where a target y^+ was used to set the near-wall spacing Δy. This target value is then specified in the passage and hub/shroud tip passages. The Reynolds number that needs to be specified is $R_{eL,}$ and the characteristic length is the chord of the blade, L. The R_{eL} parameter is hard to predict; however, a good approximation coupled with the correct turbulence models allows the boundary layer to be resolved. The y^+ should also fall between the recommended lower limit of $20 < y^+ <30$ to prevent it from falling into the vicious sub-layer (Tu, Guan-Heng, and Chaoqun, 2018).

$$\Delta y = L * \Delta y^{+}\sqrt{80}\, Re_x^{\frac{1}{14}}\, \frac{1}{Re_L} \tag{19}$$

Furthermore, a Grid Study was carried out whereby several meshes were experimented with until a suitable one was found. The correct mesh provided a satisfactory efficiency level after the solution converged. The different meshes and efficiency values are summarized in Table (6.6). Fig. (6.5) and (6.6) show the final mesh of the blade geometry designed based on 100% natural gas.

5.6 CFD Simulation

Ansys CFX was used to simulate the fluid behaviour in the turbine. The fluid properties from Tables (5.2) and (6.5) were coded into Ansys CFX-pre using guidelines proved in the relevant user guide (ANSYS, 2011). Fluid flow problems are governed by the nonlinear Navier Stokes equations, which must be solved analytically. CFD solutions can be calculated iteratively, and there are various criteria

for assessing CFD convergence, such as residual values. For each control volume, the local imbalance of a variable that is conserved is measured as residuals. The residuals can never be zero; however, the lower the value is, the greater the numerical accuracy of the solution. From the literature, a reasonable maximum residual level will be ≤ 5×10^-4, with values ≤ 4×10^-4 being considered as loosely converged (ANSYS, 2013). Convergence errors can occur by interrupting the solution algorithm or by setting high convergence tolerances (Tu, Guan-Heng, and Chaoqun, 2018). If the residual target is set too low, it can also increase the time to reach the converged solution. Thus, a convergence tolerance of 1×10^-7 was set, and a maximum iteration of 1000 was defined at this stage. The graphical user interface that was used to monitor various information about the CFD calculations and emerging solutions was the CFX solver manager.

6 Results and Discussion

6.1 Preliminary 1D design

For $\alpha_2 = 73°$, the final number of blades was calculated to be $n_r = 13$ blades. From Table (6.1), it can be observed that the resulting total-to-static efficiency was 81.8% for the case of the geometry based on 100% natural gas and using 100% natural gas as a working fluid. This geometry with working fluid constituted the preliminary design.

Table 6. 1: *Aerodynamic and Efficiency values of a 100% natural gas geometry using100% natural gas*

Parameter	Value
Impeller η_{T-T}	84.5
Impeller η_{T-s}	83.2
Stage η_{T-T}	83.0
stage η_{T-s}	81.8
Nozzle η_N	90.0
Specific speed	0.48
Rotational speed, ω	40000 [rpm]
U_2/c_0	0.69

Table 6. 2: *Impeller geometry details of a 100% natural gas geometry using100% natural gas*

Impeller Diameter, [mm]	Axial length (length/diameter)	Tip clearance/Vane height	shroud clearance	*Shroud exit/inlet radius*	*Hub exit to inlet radius*	*Mean Vane thickness at exit [mm]*
183.4	0.31	0.01	0.2	0.7	0.22	0.991

The axial length of the blade should not be too compared to the diameter of the impeller. The turbine should reduce pressure at the exit however, if the mechanism happens over a short length, there will be losses resulting from flow separation as the flow cannot cope with a sudden change in the geometry. A longer blade also means more friction drag due to more surface; however, that is a better compromise than the alternative.

Table 6. 3: *Inlet and Outlet flow parameters*

Inlet flow parameters	Value/deg	Outlet flow parameters	Value/ deg
alpha 2	73	alpha 3	-4
Beta 2	27	Beta 3	-76
M_{abs}	0.81	M_{abs}	0.171

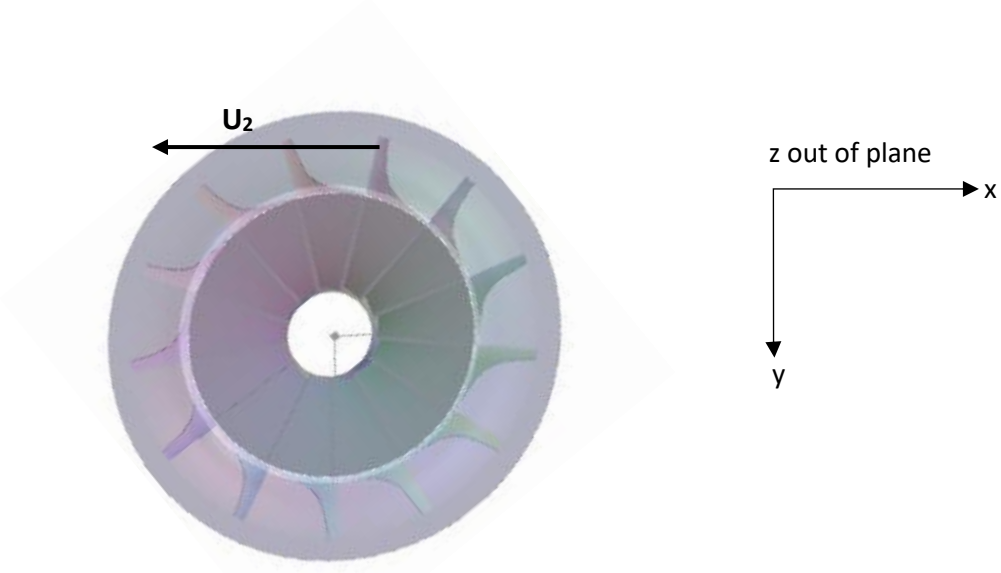

Figure 6. 5: *3D geometry of the preliminary design, showing 13 blades and direction of rotation*

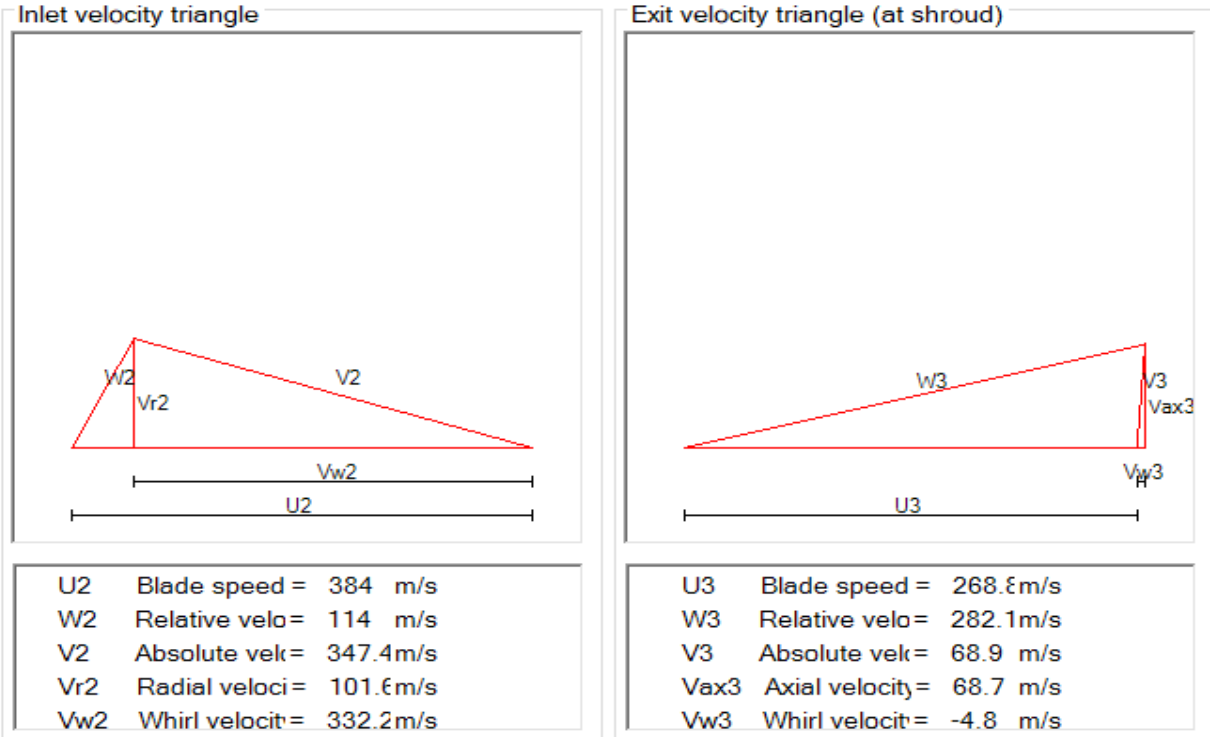

Figure 6. 6: *Velocity triangles for the inlet and outlet of the turbine for the preliminary design*

BladeGen was used to iteratively improve the flow angles by clicking and dragging the theta and beta curves. The spanwise distribution was set to radial when it was in a different setting. The spacing of the blades at the outlet was initially too narrow due to some design constraints; however some spacing was desired for aesthetics. The relative flow angle should be close to zero at the inlet, so the graph was made to start at 0°. The relative flow angle was initially -80°, and this was changed to -50° to improve the spacing between the blades.This is shown in Fig. (6.3).

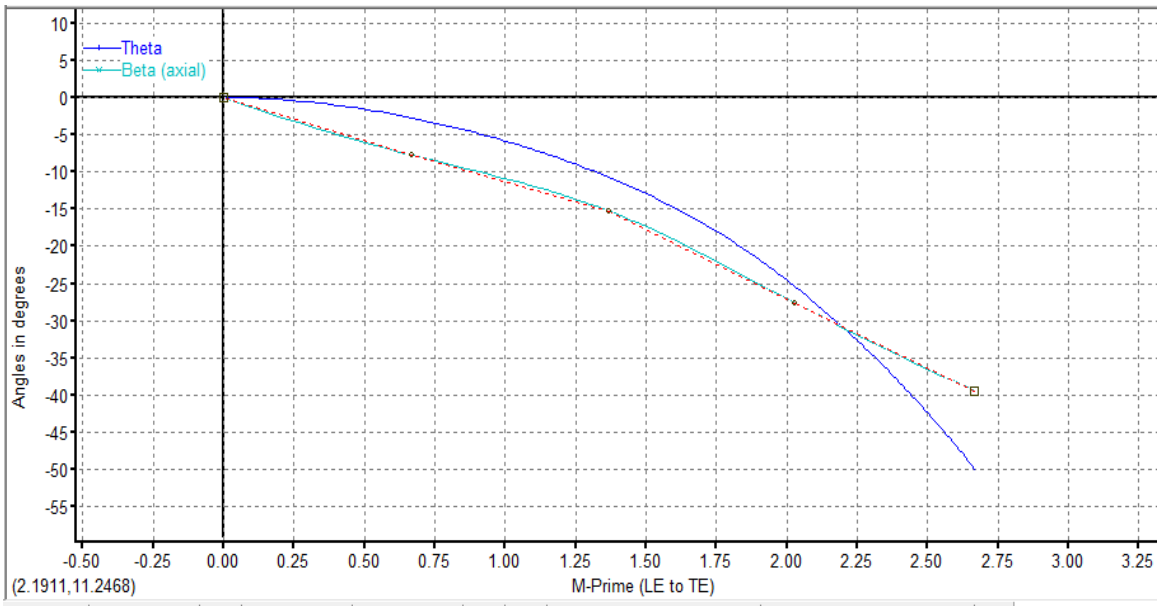

Figure 6. 7: *Theta and Beta angle plot for the preliminary design*

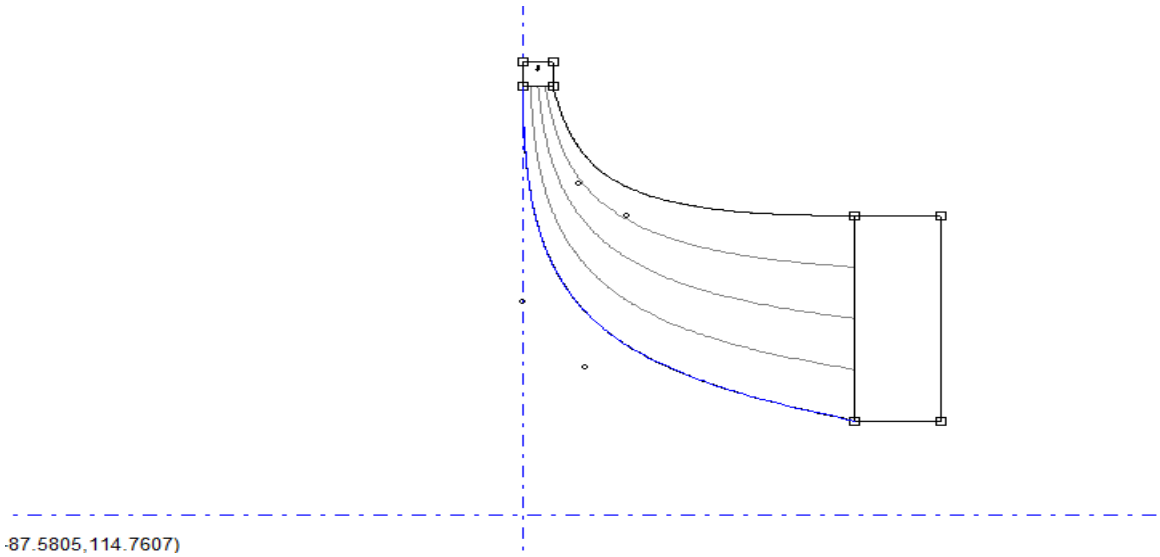

Figure 6. 8: *Final Meridional profile for preliminary design*

6.2 Energy Analysis

Table 6. 4: *Summary of Energy Analysis*

Option	T1[K]	T2[K]	$\dot{q}$ [kW]	$\dot{W}_T$ [kW]	$\dot{W}_{net}$ [kW]	ΔW [KJ/kg]
Preheat	355.9	290	1438	1696	124	11.15
Post-heat	300	236.3	1259	1494	117	10.53

From Table (6.4), a net electrical energy output is possible in both options, which is better than using an expansion valve. From this analysis, it is much more efficient to post-heat the working fluid as an extra 5.5% of energy can be extracted from the process leading to a more efficient GRS. As the temperature of 236.3K at the turbine exit is ≅ 8% below 258K, the pipes in this vicinity can be constructed from a different material compared to the rest of the pipes in the network. For instance, stainless steel can still maintain its mechanical integrity at low temperatures of $-40℃$ (Kim et al., 2015). The heating process can also begin immediately after the duct of the turbine to shorten the length of the pipe that needs this modification.

6.3 Gas Blend Cases

There are five blend cases of interest, A to E, properties of which are summarized in Table (6.5).

Table 6. 5: *Gas blend mass fraction*

Blend Case	Natural Gas Volume	Hydrogen Gas Volume	sum	X_{NG}	X_H	Sum	C_p [KJ/KgK]	R, [KJ/kgK]	ρ, [kg/m^3]
A	1	0	1	1	0	1	2.2540	0.5182	0.6680
B	0.95	0.05	1	0.9934	0.0066	1	2.3329	0.5419	0.6642
C	0.9	0.1	1	0.9862	0.0138	1	2.4197	0.5679	0.6600
D	0.85	0.15	1	0.9783	0.0217	1	2.5152	0.5964	0.6553
E	0.8	0.2	1	0.9695	0.0305	1	2.6208	0.6281	0.6502

6.4 Grid Generation and Mesh

Based on Eqn. (19) and the geometry data from Table (6.2), a Re_L value of 751819 was calculated, and a final satisfactory y^+ value of 26.4 was obtained for the preliminary design.

Table 6. 6: *Grid Study results for a single case: 100% Natural Gas Geometry*

Grid Study	Number of elements	Number of nodes	Efficiency
1	193,152	212,058	20%
2	265,384	294,480	95.60%
3	307,495	331,410	88%

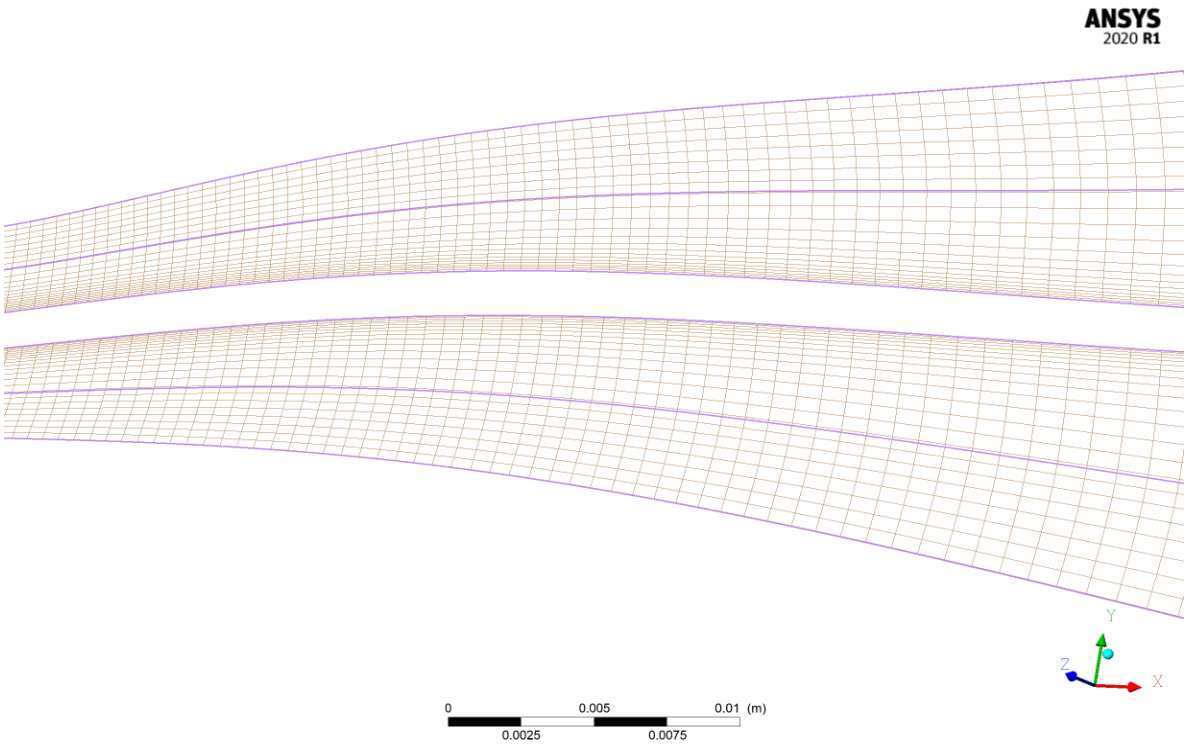

Figure 6. 9: *3D mesh of hub, revealing finer meshes near the wall and around the blade for the preliminary design*

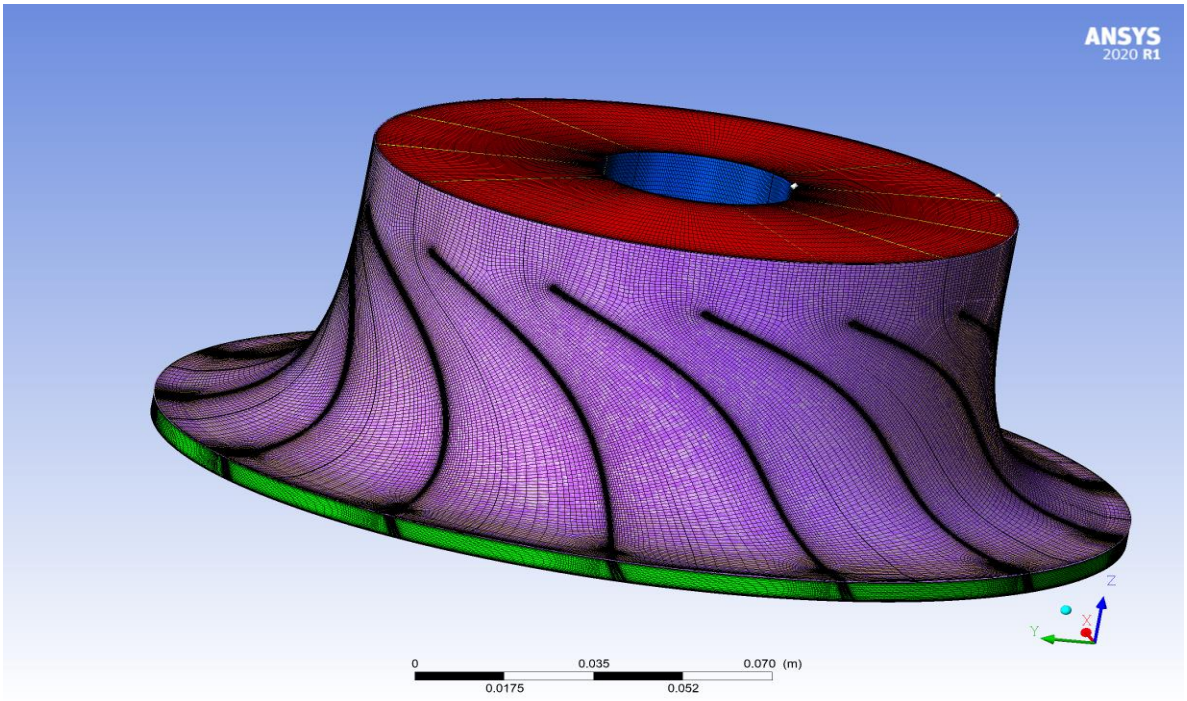

Figure 6. 10: *Mesh of complete turbine geometry optimized for blend A, using blend A as the working fluid*

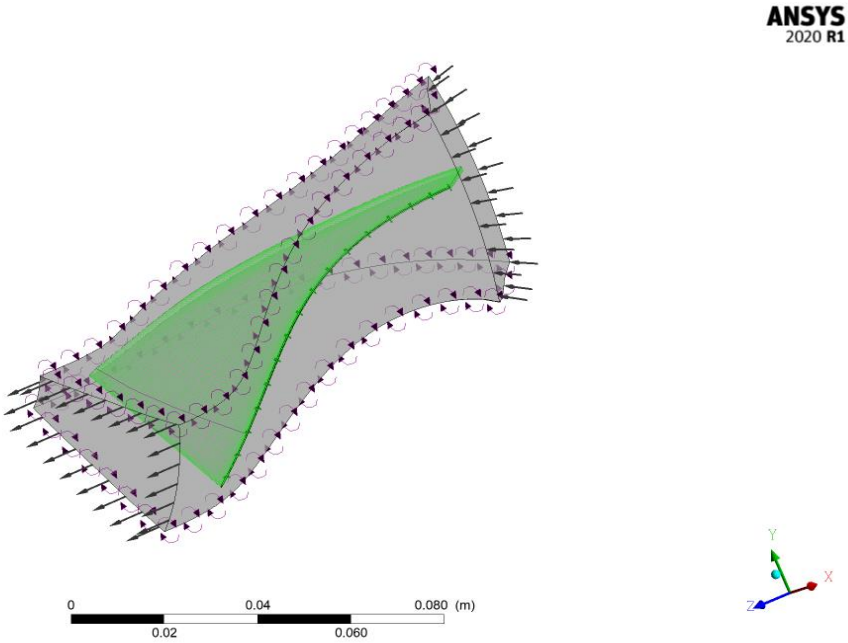

Figure 6. 11: *Computational Domain around Blade of turbine geometry optimized for blend A, using blend A as the working fluid*

6.5 CFD Simulation

The approach in determining a suitable turbine for a gas let-down station was to initially optimise five different blade designs based on the five different gas blends, A to E. Thereafter, the turbines were made to operate at off-design gas blends to determine how this would impact their respective performance. The final convergence mass and momentum residual values for the natural gas turbine design fell within acceptable limits, as shown in Fig. (7.4). A nearly straight line of the total-to-static efficiency is an indication of convergence, and once this was identified, the iteration could be stopped to save time or allowed to continue. This is shown in Fig. (7.5), and the rest of the convergence plots are placed in the appendix. The value of the efficiency at the final iteration should be used as the final solution value (ANSYS, 2013). Table 7.2 summarizes the efficiency and mass flow rate values from part one.

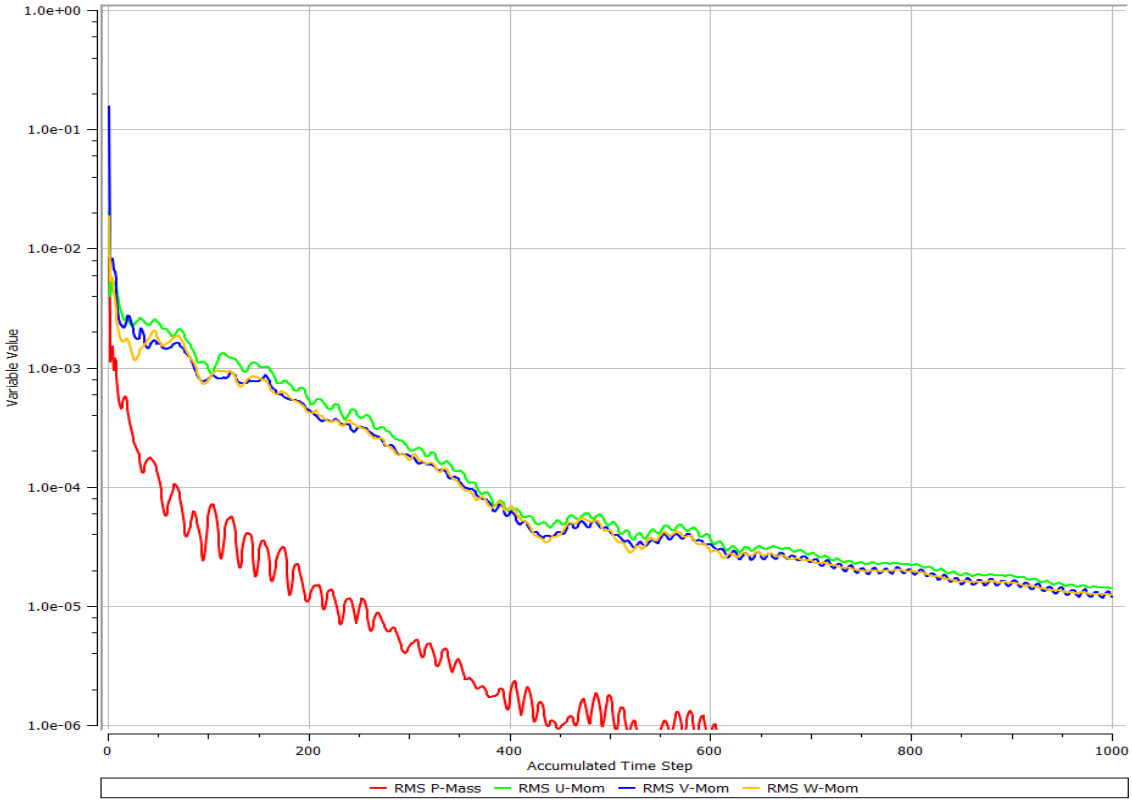

Figure 6. 12: *Mass and Momentum convergence for turbine geometry optimized for blend A, using blend A as the working fluid*

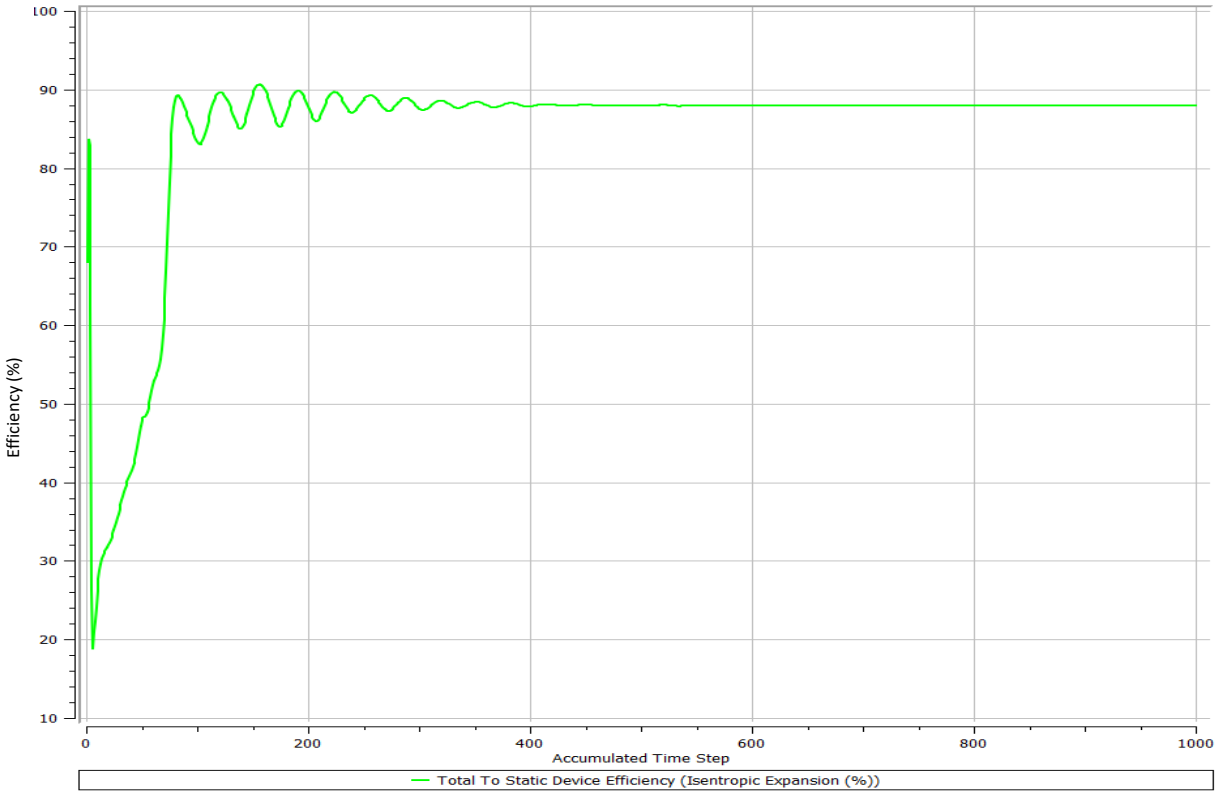

Figure 6. 13: *Efficiency convergence for turbine geometry optimized for blend A, using blend A as the working fluid*

Table 6. 7: *Summary table of all the CFD results obtained from 20 simulations*

Geometry design	A	B	C	D	E
Vista RTD efficiency	81.8	80.9	81.4	81.5	82
CFD efficiency for optimized design	88.0	81.1	74.5	73.9	73.9
% Difference of 1D vs 3D	7.6	0.2	8.5	9.3	9.9
Vista RTD mass flow rate	11.1	11.1	11.1	11.1	11.1
CFD mass flow rate	8.5	8.7	8.8	9.8	11.55
% Difference of 1D vs 3D	24.1	21.5	20.4	12.2	4.1
Average CFD efficiency based on the different blades	75.8	78.4	79.3	79.8	80.3
Average % efficiency deviation from optimum design	13.8	8.5	7.8	8.1	8.6

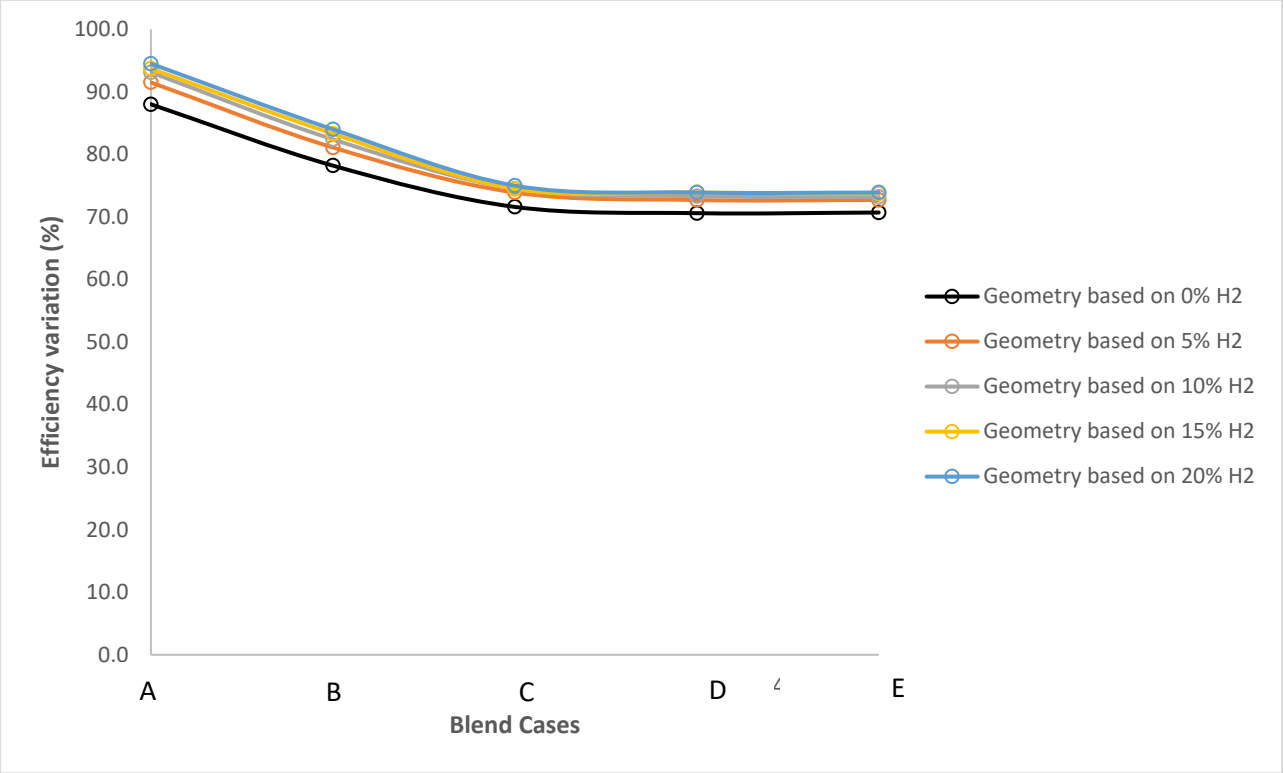

Figure 6. 14: *Efficiency variation with different blends for all the five optimized geometries*

From Fig. (6.10), a nonlinear behaviour the efficiency and the blended cases can be observed. For a given turbine geometry, the performance of the design was highest when the turbine operated on 100% natural gas. After that, there is a considerable drop in the efficiency when blend case two is used, followed by smaller decreases as the proportion of hydrogen in the mixture by volume increases. However, the efficiency for a turbine at a given gas blend was higher when the geometry was designed based on more significant percentages of hydrogen by volume. This can be seen in the vertical rise in the curves. This result shows that for a given turbine design, the machine's performance will be higher when the working fluid contains a lower percentage of hydrogen by volume. The mass flow rate values of the different geometries from the CFD results were lower than the value specified in Vista RTD, with the lowest percentage difference being attributed to the working fluid of 100% natural gas. The percent error between the CFD and the Vista RTD mass flow rate values decreased as the design of the turbine incorporated greater proportions of hydrogen.

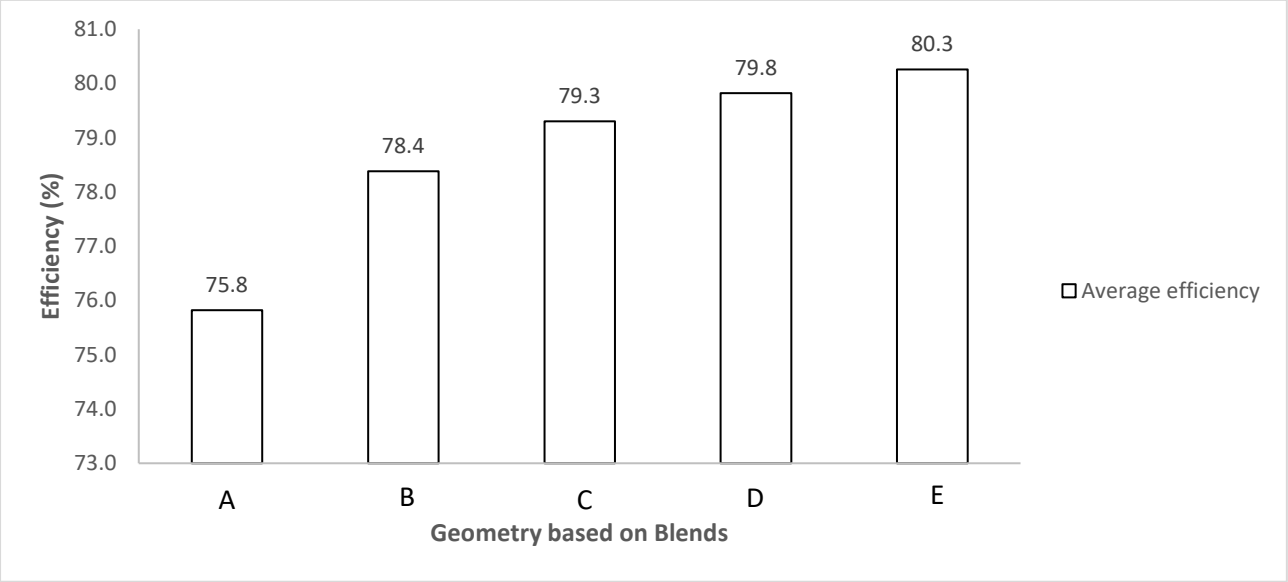

Figure 6. 15: *Average efficiency for all the five optimized geometries*

The efficiencies of all the turbines are generally high as shown in Fig. (6.11) however, the turbine with the greatest average efficiency is the one with 20% hydrogen in the blend and the lowest average efficiency is attributed to the turbine with 0% hydrogen. Between these two extremes, the average efficiency of the turbine increased when the geometric design was based on a greater amount of hydrogen in the mixture. However, the performance increases at a slower rate as the percentage of hydrogen becomes higher. The behaviour of the changes from blend cases A to E is that of an exponential decay towards a limiting value. A highly efficient turbine is important as it generally translates into extracting more energy from the working fluid and reducing losses. Based on this, geometry E is of high interest. However, an important factor to also consider is how widely the efficiencies vary from the design point, as this indicates how stable the turbine is in terms of how well it can continue to operate at a given efficiency value despite the inevitable variations of gas mixture composition.

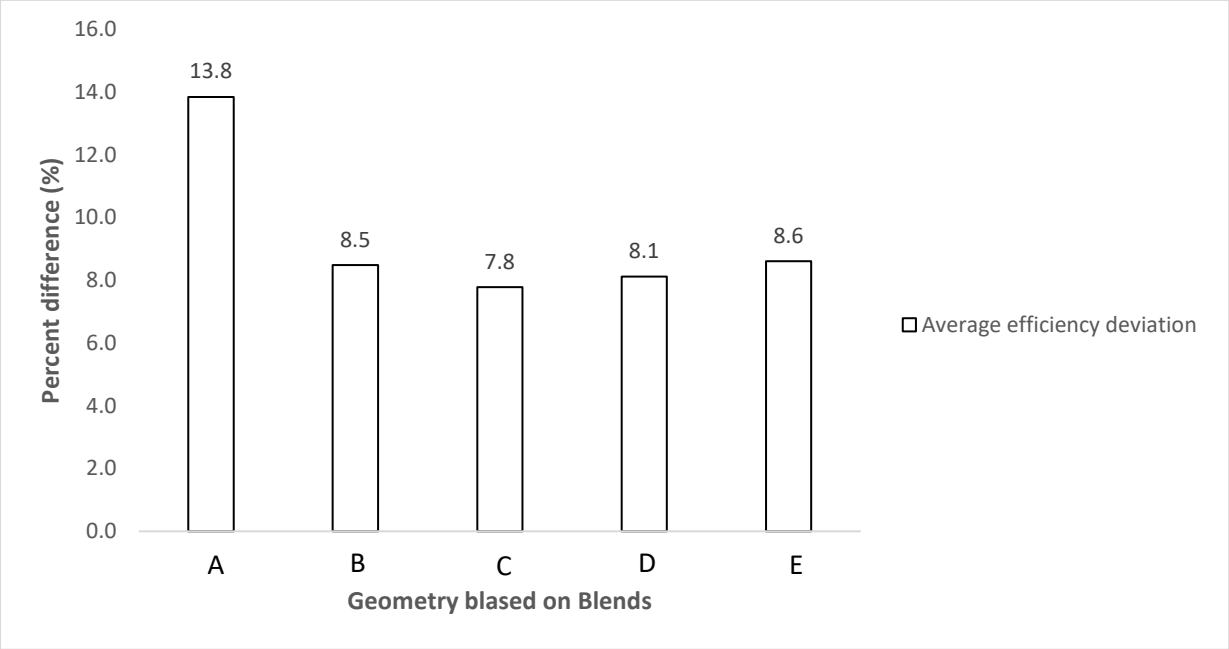

Figure 6. 16: *Average efficiency deviation for all five optimized geometries*

Over a twenty-four-hour period, the blend in the pipeline can vary from blend cases A to E. Suppose each blend is available for 24/5 ≅ 5 hours, the efficiency of a given turbine will also vary accordingly. Thus, the overall isentropic efficiency of the turbine can be assumed to be the average of the variation. The different geometries designed based on blend cases A to E will yield different averages.

Fig. (6.12) shows that the deviation from the design point was not uniform across all the geometries. The geometry based on gas blend A had the most variation at an average of 13.8%. However, the lowest deviation did not correspond to the turbine with the greatest efficiency value. The geometry based on gas blend C had the lowest deviation, meaning that it is more stable on average than the other turbines. Unlike the average efficiency variation, the behaviour of the changes from A to E cannot be described by a mathematical function. Based on this observation, the recommended turbine design for the GRS in the Czech Republic is based on geometry C, with an average efficiency of 79.3%. This is because it is ≅ 10.3% more stable and only 1.3% less efficient than the geometry based on blend E, which had the highest efficiency of 80.3%. The final geometry based on blend C is shown in Fig. (6.13). Since this geometry has a 90:10 natural gas to hydrogen ratio, it provides decarbonization benefits while maintaining high efficiency. To make a more accurate recommendation, it would be helpful to have a model that predicts blend variation in a gas grid and couple the results obtained with that data.

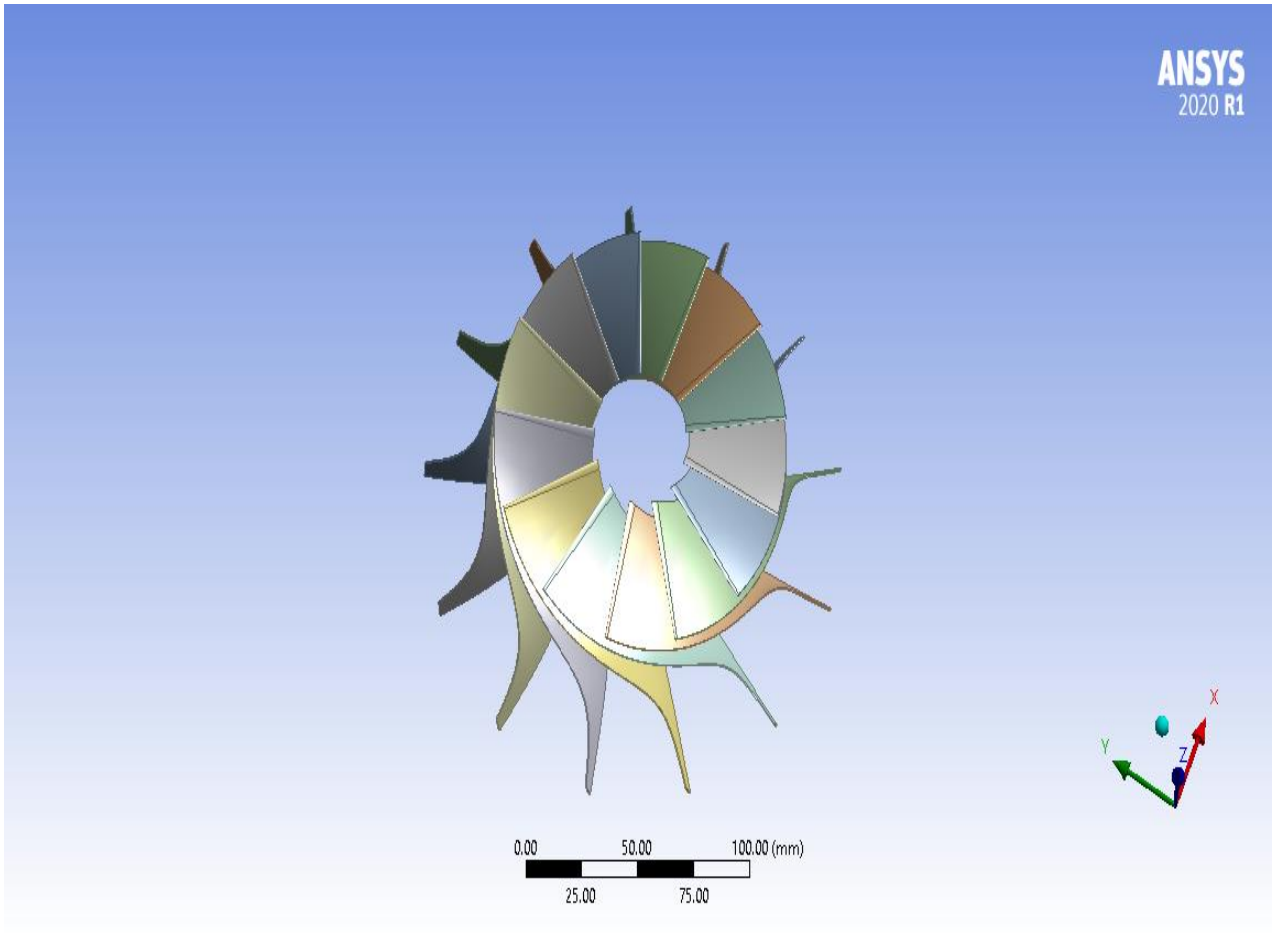

Figure 6. 17: *Geometry of final design showing all 13 blades crested from the 90% methane and 10% hydrogen gas blend, obtained from Design Modeler.*

Different countries impose different limits on the content of hydrogen in a natural gas pipeline system, which is driven by technical conditions for a given pipeline. Hydrogen content in natural gas deteriorates the energy content and has an adverse effect on the calorific value of natural gas, which explains the decrease in efficiency values for the blended cases. Some European countries have imposed a limit of 0.1 to 12% of hydrogen by volume (Kuczynski et al., 2019b). Another benefit of adding hydrogen into the natural gas pipeline is reducing natural gas pressure drop when its being transported, which can enable transportation over longer distances since no additional compressor stations will be needed.

7 Conclusion and Recommendations

This research presented a complete design process for an IFR turbine that can be made to operate at a typical gas let-down station. The design process entailed a preliminary 1D design using Vista RTD followed by an extensive CFD analysis using Ansys CFX, the results of which were compared. The best turbine performance was seen in the geometric design based on 20% hydrogen however, the design based on 10% hydrogen is recommend as an approach to design a turboexpander in a future where hydrogen gas becomes more prevalent in the gas pipelines. This design can enable higher penetration of renewables into the gas grid without significantly modifying the existing infrastructure.

The analysis results and final recommendations are provided based on the quality of the 1D design and CFD simulations. For a fraction of the simulations, the disparity between the efficiency values was over 10% thus, further research is required to determine whether the analysis can be improved in Vista RTD and/or CFD. Further iterations on the rotational could have also been carried out to improve the efficiency of some the results obtained from this investigation. The techniques for CFD could also be improved to achieve a finer mesh. While all the necessary simulations were carried out, the pressure distribution and vorticities could not be verified due to a problem with CFX. Although such details were out of the scope of the project, this issue could be fixed to provide further insights into the flow structure inside the turbine. One of the challenges was in finding a typical prediction of the variation of the blend throughout the day, seasons as well geographically, as that can also vary.

8 Limitations

As mentioned in the methodology section, a turbine consists of various components thus, a detailed aerodynamic design for the holistic turbine could have provided a more accurate evaluation of the performance. Transient effects were not analysed thus, the effect of variable flow rates on the performance of the turboexpander could have been investigated. An assessment of the environmental benefits could have also been carried out to assess the efficacy of the design in reducing the carbon footprint of gas reduction stations.

9 Bibliography

ANSYS, I. (2011). *ANSYS CFX-Pre User's Guide*, 14th ed. Canonsburg: ANSYS.

ANSYS, I. (2013). *ANSYS CFX Solver Manager User's Guide*, 15th ed. Canonsburg: ANSYS.

ANSYS, I. (2015). *ANSYS TurboGrid User's Guide*, 17th ed. Canonsburg: ANSYS.

Balmer and Robert T. (2011). *Modern Engineering Thermodynamics*.

Dixon, S.L. and Hall, C.A. (2010). *Fluid Mechanics and Thermodynamics of Turbomachinery*.

Dodds, P.E. and McDowall, W. (2013). The future of the UK gas network. *Energy Policy*, 60, 305–316. Available from https://doi.org/10.1016/j.enpol.2013.05.030. [Accessed 28 October 2021].

Farzaneh-Gord, M. et al. (2012). Feasibility of accompanying uncontrolled linear heater with solar system in natural gas pressure drop stations. *Energy*, 41 (1), 420–428. Available from https://doi.org/10.1016/j.energy.2012.02.058. [Accessed 4 November 2021].

Glassman, A. (1976). *COMPUTER PROGRAM FOR DESIGN ANALYSIS OF RADIAL-INFLOW TURBINES*. Ohio. Available from https://ntrs.nasa.gov/citations/19760010058 [Accessed 4 March 2022].

Kim, J.H. et al. (2015). Charpy impact properties of stainless steel weldment in liquefied natural gas pipelines: Effect of low temperatures. *Materials and Design*, 65, 914–922. Available from https://doi.org/10.1016/j.matdes.2014.09.085 [Accessed 1 April 2022].

Kuczynski, S. et al. (2019a). Techno-economic assessment of turboexpander application at natural gas regulation stations. *Energies*, 12 (4). Available from https://doi.org/10.3390/en12040755. [Accessed 6 March 2022].

Kuczynski, S. et al. (2019b). Thermodynamic and technical issues of hydrogen and methane-hydrogen mixtures pipeline transmission. *Energies*, 12 (3). Available from https://doi.org/10.3390/en12030569. [Accessed 1 November 2021].

Maddaloni, J.D. and Rowe, A.M. (2007). Natural gas exergy recovery powering distributed hydrogen production. *International Journal of Hydrogen Energy*, 32 (5), 557–566. Available from https://doi.org/10.1016/j.ijhydene.2006.06.039 [Accessed 24 April 2022].

Melaina, M.W., Antonia, O. and Penev, M. (2013). *Blending Hydrogen into Natural Gas Pipeline Networks: A Review of Key Issues*. Available from http://www.osti.gov/bridge. [Accessed 14 December 2021].

Michal, T. (2013). *ANSYS_TurboSystem_Users_Guide (1)*, 15th ed. Canonsburg: ANSYS.

Morgese, G. et al. (2020). Fast design procedure for turboexpanders in pressure energy recovery applications. *Energies*, 13 (14). Available from https://doi.org/10.3390/en13143669. [Accessed 4 January 2022].

Neseli, M.A., Ozgener, O. and Ozgener, L. (2015). Energy and exergy analysis of electricity generation from natural gas pressure reducing stations. *Energy Conversion and Management*, 93, 109–120. Available from https://doi.org/10.1016/j.enconman.2015.01.011. [Accessed 4 February 2022].

Poživil, J. (2004). *Use of Expansion Turbines in Natural Gas Pressure Reduction Stations*.

Rohlik, H. (1968). *Analytical determination of radial inflow turbine design geometry for maximum efficiency*. Ohio: NASA.

Sam, A.A. and Ghosh, P. (2017). Flow field analysis of high-speed helium turboexpander for cryogenic refrigeration and liquefaction cycles. *Cryogenics*, 82, 1–14. Available from https://doi.org/10.1016/j.cryogenics.2017.01.004. [Accessed 4 April 2022].

Szoplik, J. (2012). *The Gas Transportation in a Pipeline Network*. Available from www.intechopen.com. [Accessed 4 December 2021].

Tu, J., Guan-Heng, Y. and Chaoqun, L. (2018). *Computational Fluid Dynamics, A Practical Approach*, 3rd ed.

Villecco, F. and Pellegrino, A. (2010). Design optimization of a natural gas substation with intensification of the energy cycle. *Mathematical Problems in Engineering*, 2010. Available from https://doi.org/10.1155/2010/294102. [Accessed 17 December 20221.

Whitfield, A. and Baines, N. (1990). *Design of Radial Turbomachines*. United States.

Witkowski, A. et al. (2018). Analysis of compression and transport of the methane/hydrogen mixture in existing natural gas pipelines. *International Journal of Pressure Vessels and Piping*, 166, 24–34. Available from https://doi.org/10.1016/j.ijpvp.2018.08.002. [Accessed 24 October 2021].

10 Appendix

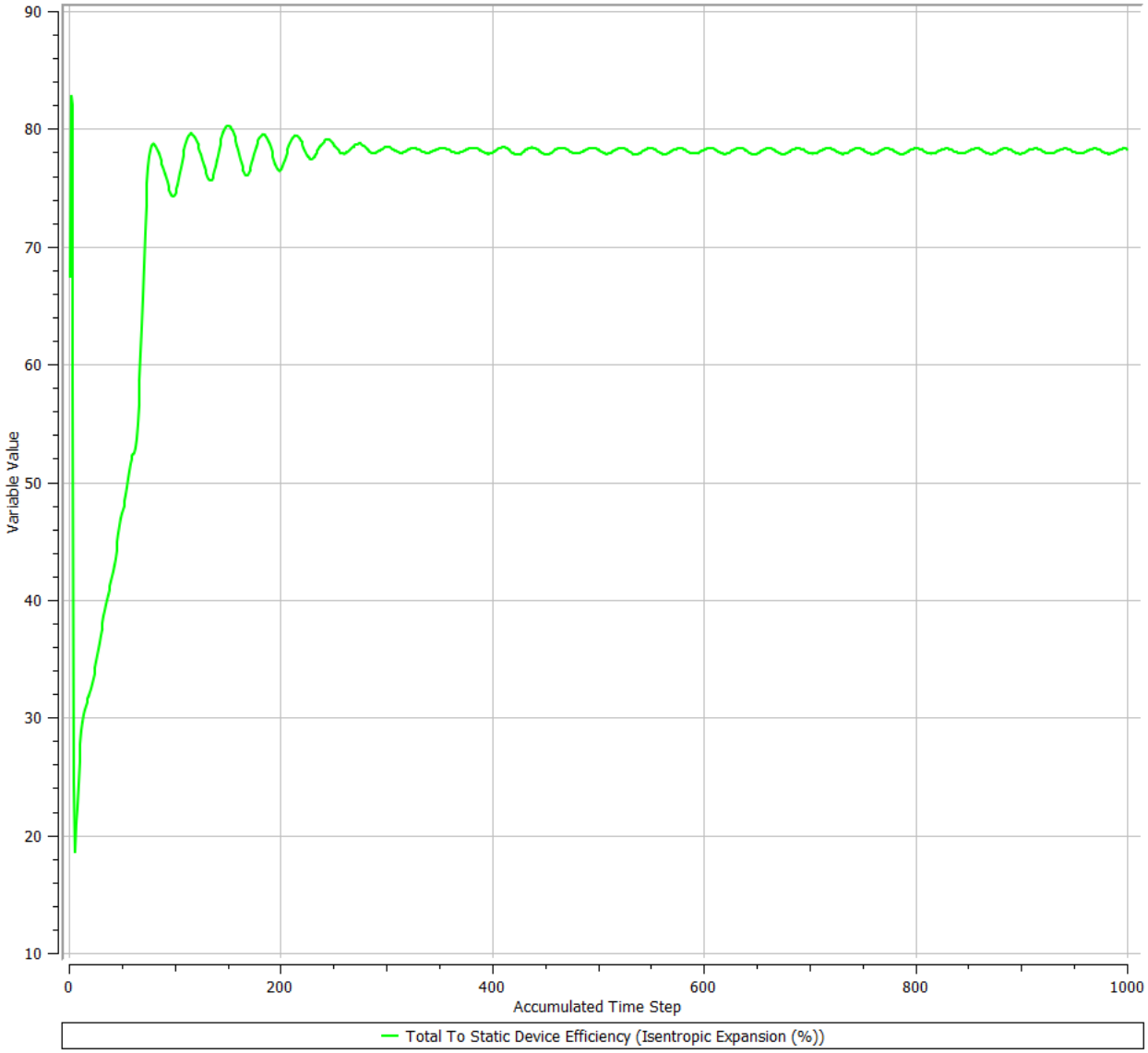

Figure 10. 1: *Efficiency convergence for turbine geometry optimized for blend A, using blend B as the working fluid*

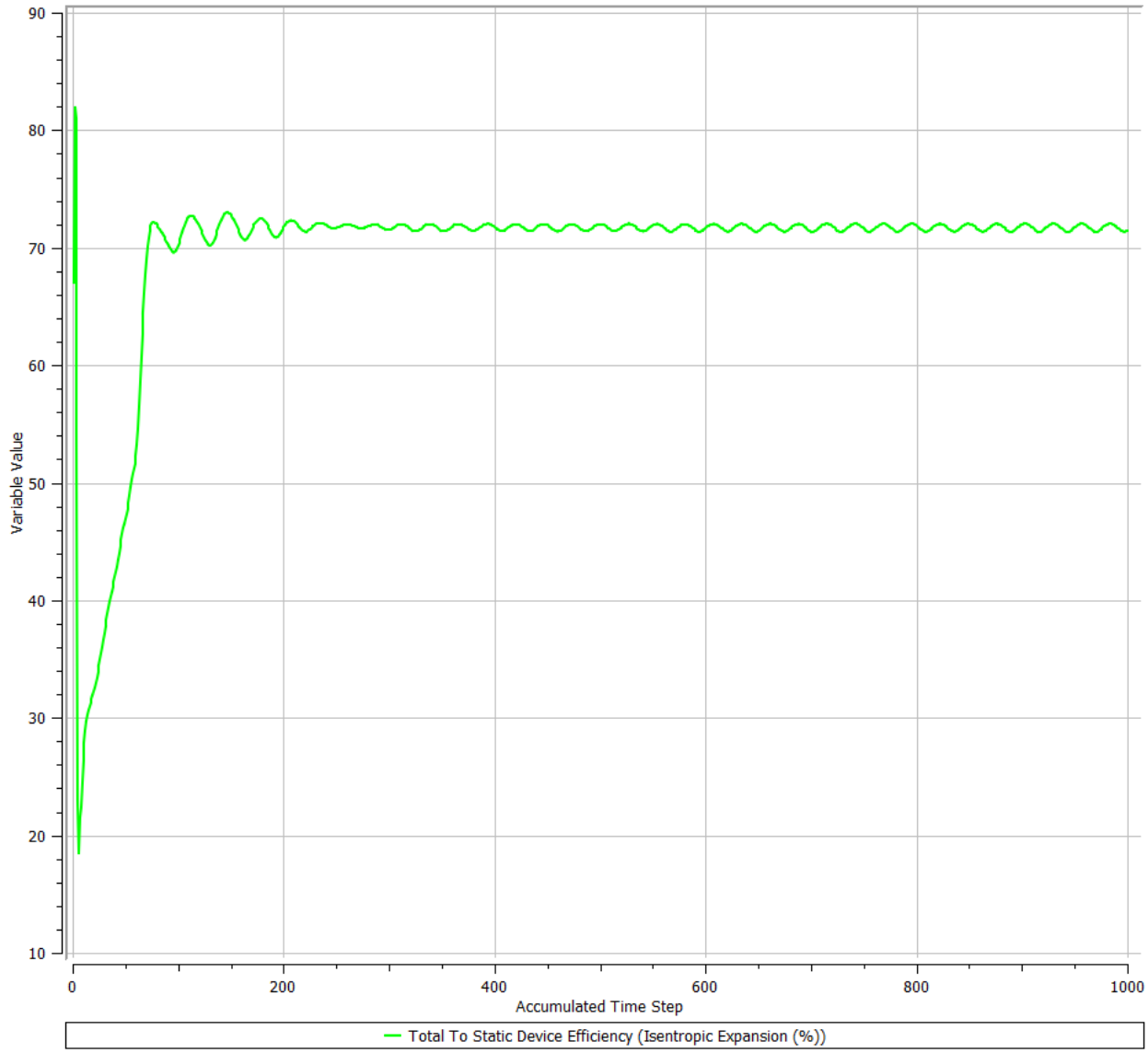

Figure 10. 2: *Efficiency convergence for turbine geometry optimized for blend A, using blend C as the working fluid*

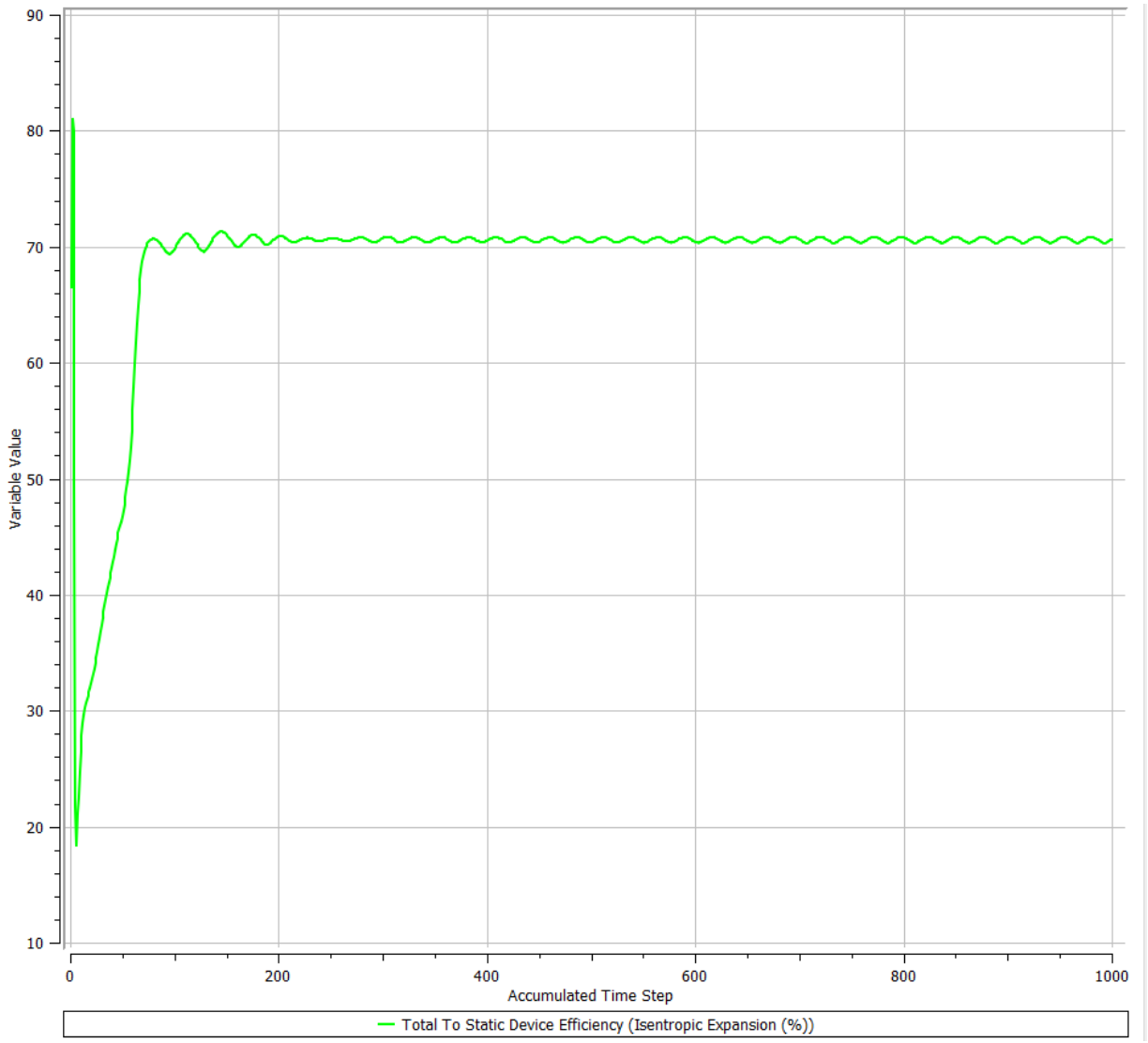

Figure 10. 3: *Efficiency convergence for turbine geometry optimized for blend A, using blend D as the working fluid*

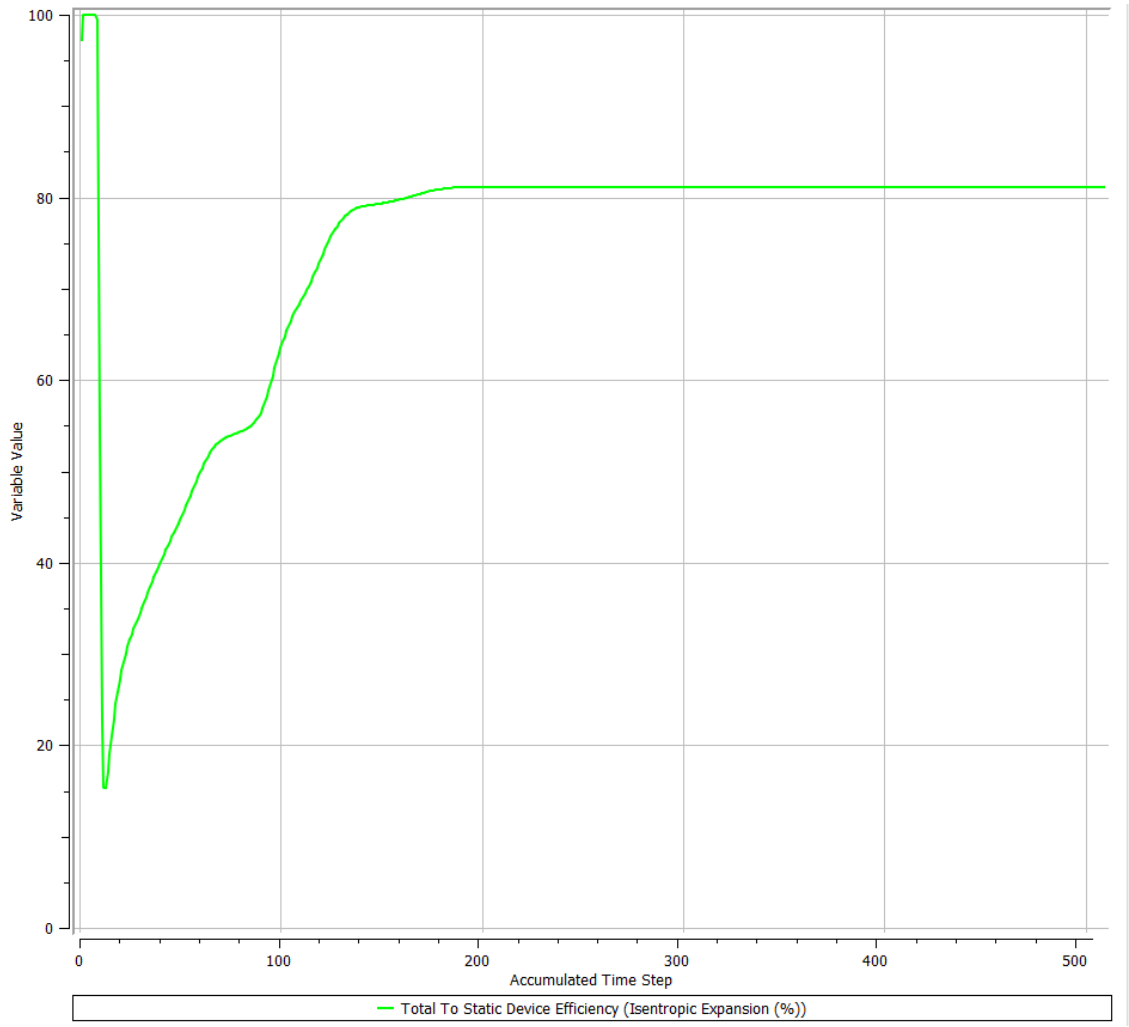

Figure 10. 4: *Efficiency convergence for turbine geometry optimized for blend B, using blend B as the working fluid*

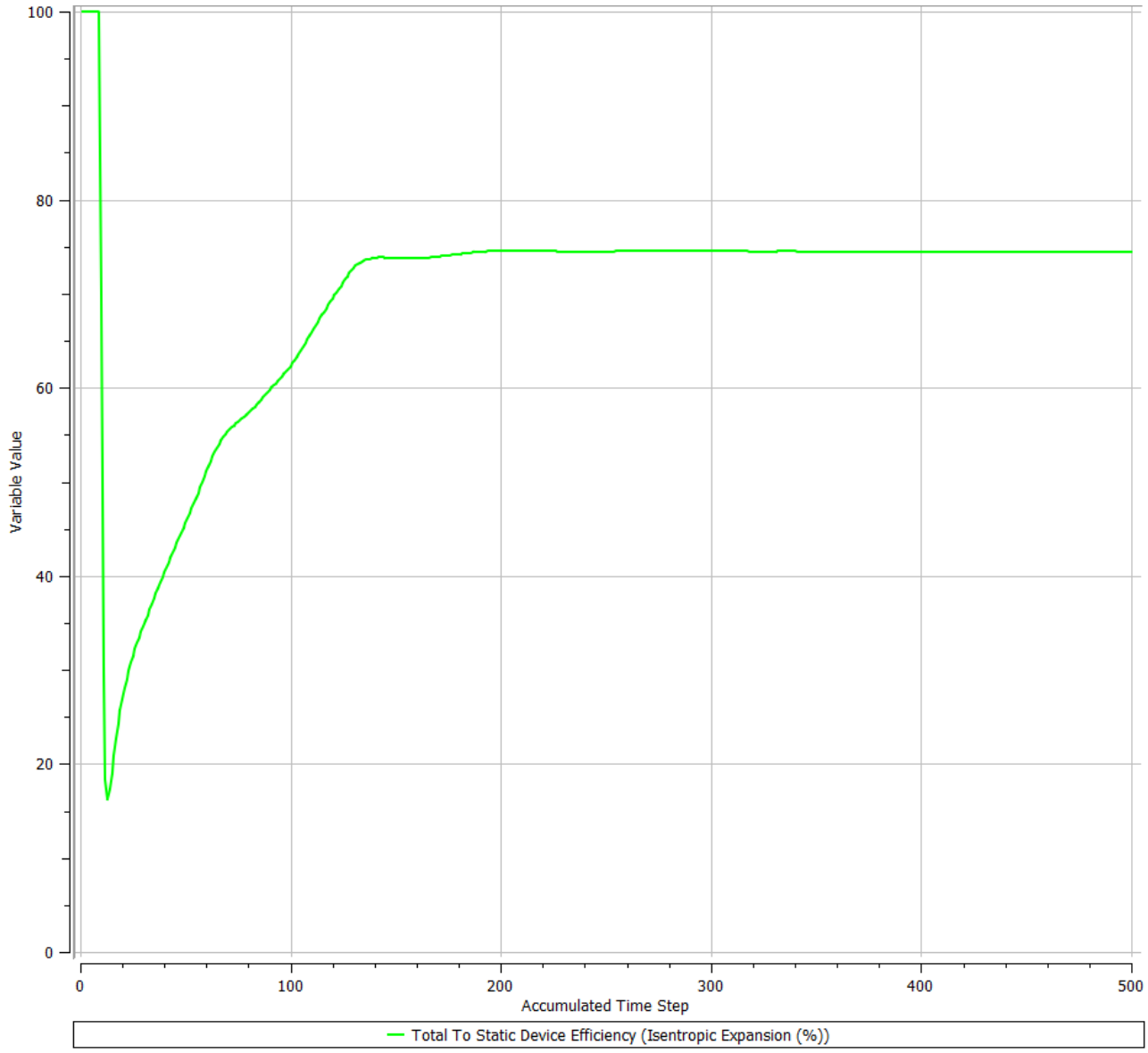

Figure 10. 5: *Efficiency convergence for turbine geometry optimized for blend C, using blend C*

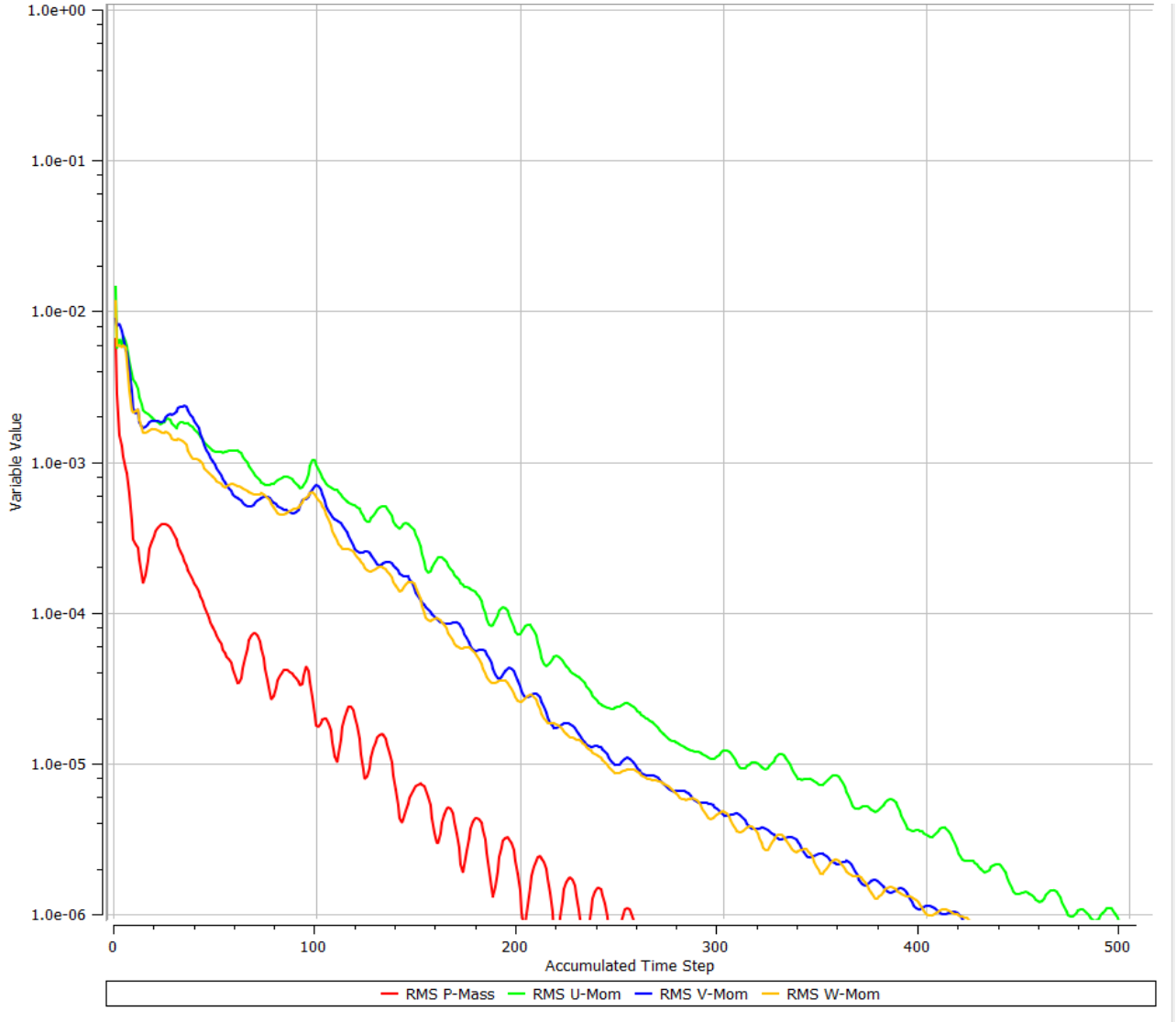

Figure 10. 6: *Mass and Momentum convergence for turbine geometry optimized for blend C, using blend C*

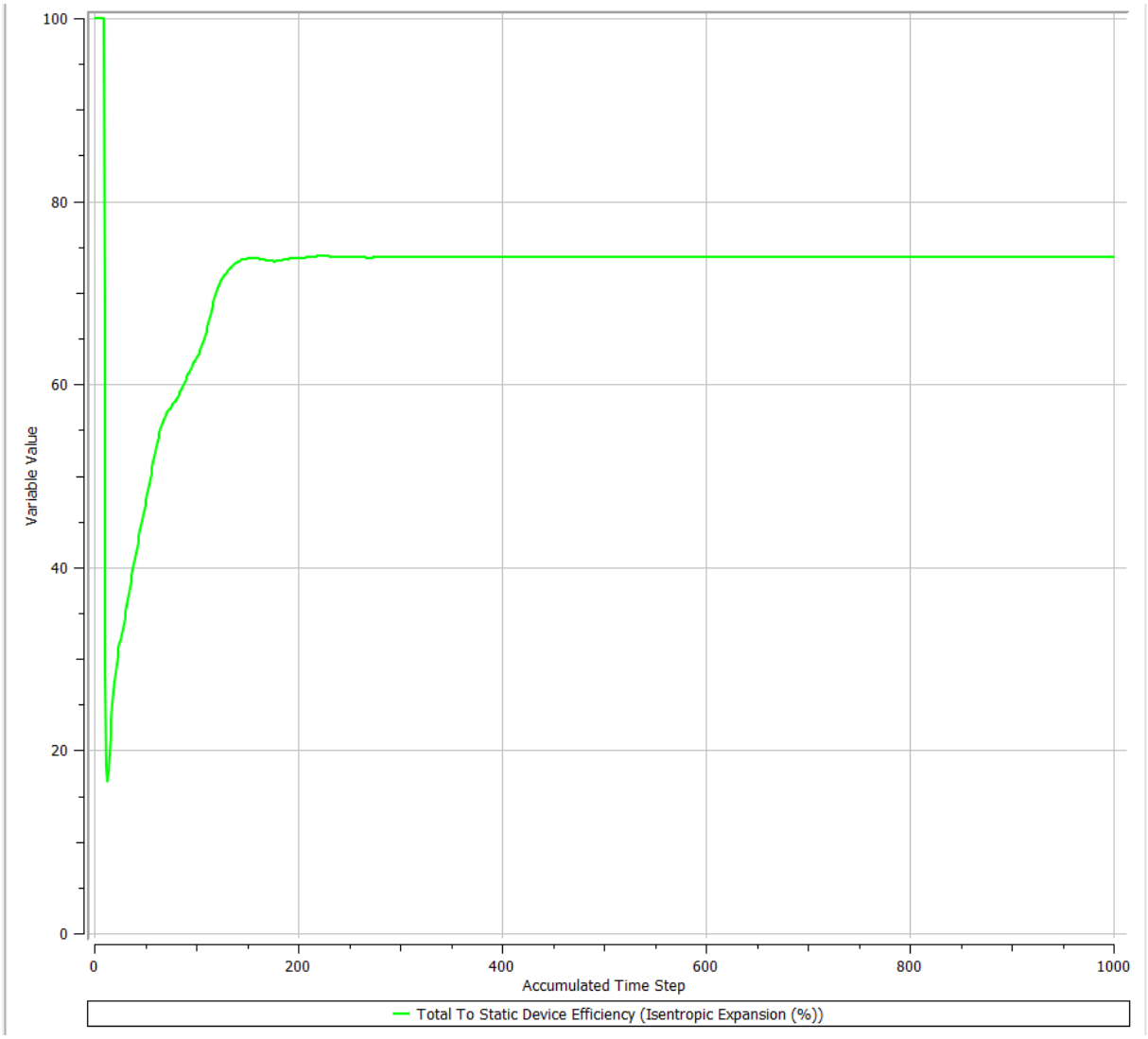

Figure 10. 7: *Efficiency convergence for turbine geometry optimized for blend D, using blend D*

```
clear
close all
clc
%% Which requires less energy Pre-heating or Post heating?
% Initialisation
eta = 0.8; %isentropic efficiency
eta2 = 0.97; % gearbox or mechanical
eta3 = 0.95; % efficeicy of generator
m_dot = 11.13; %kg/s
T2 = 290;  %k and equal to T_out lower due to losses in pipes
R_methane = 0.5182; %KJ/Kg.K
M_methane = 16.043; %Molecular weight of methane gas in Kg/Kmol
%defining constants for Methane valid for T (K): 273<T<1500
a = 19.89;
b = 5.024e-2;
c = 1.269e-5;
d = -11.01e-9;
%Cp Polynomial (Temperature)Function: Max % error:1.33 Avg. = 0.57
c_p1 = a+b*T2+c*T2^2+d*T2^3; %KJ/kmolK
c_p1_corrected = c_p1/M_methane; %KJ/kgK
%Boundary conditions of Turbine
p1 = 5.5e6;
p2 = 1.8e6;
c_v1 = c_p1_corrected - R_methane;
k = c_p1_corrected/c_v1;
w = (p2/p1)^((k-1)/k);
T1 = T2/(eta*(w-1+(1/eta))) % Preheat temp where w is just a constant
%Heat Calculation
%Cp Polynomial (Temperature)Function: Max % error:1.33 Avg. = 0.57
T_avg = (T1+T2)/2;
c_p_avg = a+b*T_avg+c*T_avg^2+d*T_avg^3; %KJ/kmolK
c_p_avg_corrected = c_p_avg/M_methane;
Qin_pre = m_dot*c_p_avg_corrected*(T1-300) %kw t2 should be Tin
% which is 300k! (T1 -Tin) T1 is 355.9K
```

Figure 10. 8: *MATLAB code for energy analysis, PART 1*

```
%% For post heating
T1_new = 290; %K %tout
%Cp Polynomial (Temperature)Function: Max % error:1.33 Avg. = 0.57
c_p2 = a+b*T1_new+c*T1_new^2+d*T1_new^3;%KJ/kmolK
c_p2_corrected = c_p2/M_methane; %KJ/kgK
%Boundary conditions of Turbine
p1 = 5.5e6;
p2 = 1.8e6;
c_v2 = c_p2_corrected - R_methane;
k_new = c_p2_corrected/c_v2;
w2 = (p2/p1)^((k_new-1)/k_new);
T2_new = T1_new*eta*(w2-1+(1/eta)) % T2
T_avg2 = (T1_new+T2_new)/2;
c_p2_avg = a+b*T_avg2+c*T_avg2^2+d*T_avg2^3; %KJ/kmolK
c_p2_avg_corrected = c_p2_avg/M_methane;
Qin_post = m_dot*c_p2_avg_corrected*(T1_new-T2_new)%kw should be (Tout -T2)
% Tout is 290K and T2 is 236.3K

%%  Turbine power output
Wt1 = m_dot*c_p_avg_corrected*(T1-T2) %Turbine power, where t1 is 355.9k
%and t2 is 290K
Wt2 = m_dot*c_p2_avg_corrected*(300-T2_new)% t1 is tout which is 300K
% and T2 is 290 and t2_new is 236.3k (Tout - T2)

%% Net Electric power total electric - heat required
Wnet_preheat = eta2*Wt1*eta3 - Qin_pre
Wnet_postheat= eta2*Wt2*eta3 - Qin_post

%% Specific Power
wnet_dot_preheat = Wnet_preheat/m_dot
wnet_dot_postheat = Wnet_postheat/m_dot
```

Figure 10. 9: *MATLAB code for energy analysis, PART 2*

```
clear
close all
clc
%% Mass Fraction Calculations
%Initialisation
R =8.3143; %kj/kgmole*K
M_m =16.043; %kg/kmol
M_h =2.016; %kg/kmol
K_m =1.299;
K_h =1.405;
rho_m =0.668;
rho_h =0.08375;
%these are the mole fractions given as volumes
Vol_m = 0.85;
Vol_h = 0.15;
Sum_1 = Vol_m+Vol_h
%S1.Equivalent molecular mass of mixture
M_eqv = M_m*Vol_m +M_h*Vol_h;
%S2.Mixture composition on Mass basis
X_m = Vol_m*(M_m/M_eqv)
X_h = Vol_h*(M_h/M_eqv)
Sum_2 = X_h+X_m
%S3.Determine R_mixture
R_eqv = R/M_eqv
```

```
%S2.Mixture composition on Mass basis
X_m = Vol_m*(M_m/M_eqv)
X_h = Vol_h*(M_h/M_eqv)
Sum_2 = X_h+X_m
%S3.Determine R_mixture
R_eqv = R/M_eqv
R_eqv2 = X_m*0.5182 +X_h*4.124
%S4.Determine cp_mixture
Cp_eqv = X_m*2.2537 +X_h*14.307
%S5.Determine rho_mixture
rho_eqv = X_m*rho_m +X_h*rho_h
```

Figure 10. 10: *MATLAB code for mass fraction calculation*